Università degli Studi di Padova

Dipartimento di Salute della Donna e del Bambino

Corso di Dottorato in Medicina dello Sviluppo e

Scienze della Programmazione Sanitaria

XXXII° ciclo

Curriculum in: Emato-oncologia, genetica, malattie rare e medicina predittiva

Recellularized colorectal patient-derived scaffold as *in vitro* pre-clinical 3D model for drug screening

Tesi di dottorato redatta con il contributo finanziario di
Istituto di Ricerca Pediatrica Città della Speranza

Coordinatore: Ch.mo Prof. Carlo Giaquinto

Supervisore: Ch.mo Prof. Gianni Bisogno

Co-supervisore: Dott. Marco Agostini

Dottorando: Francesca Sensi

INDEX

ABBREVIATIONS

2D: two-dimensional

3D: three- dimensional

3DN: recellularized three-dimensional normal tissues

3DT: recellularized three-dimensional tumor tissues

5-FU: 5-Fluorouracil

AJCC: American Joint Committee on Cancer

APC: adenomatous polyposis coli

CIN: chromosomal instability

CRC: colorectal cancer

AQP: aquaporins

DAPI: 4',6-diamidino-2-phenylindole

DET: detergent-enzymatic treatment

ECM: extracellular matrix

EDU: 5-ethynyl-2'-deoxyuridine

EGFR: epidermal growth factor receptor

EHS: engelbreth-holm-warm

EXPeRT: European Cooperative Study Group for Pediatric Rare Tumors

FA: folinic acid

FAP: familial adenomatous polyposis

FOLFOX: 5-fluorouracil + oxaliplatin + folinic acid

FOLFIRI: 5-fluorouracil+ irinotecan+ folinic acid

HE: haematoxylin and eosin

HNPCC: hereditary non-polyposis colorectal cancer

IC50: the half maximal inhibitory concentration

IF: immunofluorescence

IHC: immunohistochemistry

MAP: MUTYH-associated polyposis

MHC-II: histocompatibility complex type II

MHs: macroporous hydrogels

MSI: microsatellite instability

OCT: optimal cutting temperature compound

PDMS: polidimetilsilossano

PBS: phosphate buffered saline

PCL: polycaprolactone

PLA: polylactic acid

PGA: polyglycolic acid

PLGA: polylactic-co-glycolide

PVDF: polyvinylidine fluoride

qRT-PCR: quantitative reverse transcription polymerase chain reaction

SDC: sodium deoxycholate

SEM: scanning electron microscopy

TREP: Rare Tumors in Pediatric Age

SOMMARIO

Scopo: Il carcinoma del colon-retto (CRC), è il terzo tumore più comunemente diagnosticato in uomini e donne e mostra una gestione terapeutica altamente inefficace. Al contrario, il CRC è un tumore pediatrico raro, che rappresenta solo l'1% di tutte le neoplasie pediatriche, con un'incidenza di circa uno per milione. In questo contesto, un'urgente necessità non ancora affrontata è l'assegnazione random del trattamento chemioterapico adiuvante in pazienti affetti da carcinoma del colon in stadio II e stadio III ad alto rischio, sia giovani che adulti, senza alcun fattore predittivo di efficacia. In secondo luogo, nel campo dell'identificazione di nuovi farmaci, la fase critica è la valutazione preclinica di citotossicità, efficacia ed efficienza dei farmaci. Intendiamo sviluppare un modello preclinico tridimensionale (3D) derivato dal paziente utile per la valutazione dei farmaci in grado di mimare *in vitro* la malattia del paziente.

Metodi: La mucosa del colon sano e la controparte tumorale, sono stati resecati chirurgicamente e decellularizzati secondo il trattamento detergente-enzimatico (DET). La matrice extracellulare DET è stata ricellularizzata con cellule HT29. La caratterizzazione qualitativa e quantitativa dei campioni ricellularizzati è stata valutata attraverso tecniche di istologia, immunofluorescenza e quantificazione del DNA. Il test di chemosensibilità è stato eseguito utilizzando una concentrazione crescente di 5-fluorouracile (5-FU), nell'intervallo compreso tra 0,1 µM e 100 µM. Sono stati condotti studi *in vivo* usando il modello animale zebrafish (*Danio rerio*). Per i saggi nel modello xenotrapianto, le cellule HT29 sono state iniettate nel condotto di Couvier e successivamente incubate in piastre da 96 pozzetti con diverse concentrazioni di 5-FU. L'assorbimento e la perfusione dei farmaci attraverso le matrici extracellulari tumorali

fresche e DET sono stati valutati qualitativamente per mezzo dell'autofluorescenza della doxorubicina (doxo, 594nm) e quantitativa applicando la Legge di Darcy. I monociti estratti da buffy coat, sono stati coltivati con le matrici DET e marcatori caratteristici dei macrofagi sono stati valutati in citometria a flusso.

Risultati: Il protocollo di decellularizzazione ha permesso di preservare la struttura e l'ultrastruttura originale dei tessuti (analisi SEM). Cinque giorni dopo la ricellularizzazione con la linea cellulare HT29, il modello 3D CRC ha mostrato una sensibilità ridotta ai trattamenti con 5-FU rispetto alla coltura 2D convenzionale. L'IC50 calcolato risulta 11,5 µM e 1,3 µM di 5-FU, rispettivamente. Nel modello di xenotrapianto di zebrafish, la extravasazione delle HT29 è stato rilevata dopo 4 giorni dall'iniezione. Inoltre, abbiamo ottenuto un IC50 di 5-FU completamente comparabile a quella osservata nel modello CRC 3D. Usando la microscopia confocale, abbiamo dimostrato che la doxorubicina si diffonde attraverso il volume del modello CRC 3D e co-localizza con i nuclei cellulari che ripopolano la

matrice CRC 3D. Infine, abbiamo osservato che i monociti esposti alla matrice decellularizzata tumorale si sono differenziati verso un profilo antinfiammatorio simile ai macrofagi pro-tumorali.

Conclusione: Il modello 3D CRC potrebbe essere uno strumento preclinico affidabile per colmare il divario tra i test di sperimentazione farmacologica *in vitro* e *in vivo*. Il modello 3D CRC, tradotto in ambito pediatrico, potrebbe aiutare i medici e gli oncologi a identificare il trattamento più adatto per il paziente.

ABSTRACT

Purpose: Colorectal cancer (CRC), the third most common cancer diagnosed in both men and women shows a highly ineffective therapeutic management. In contrast, CRC is a rare pediatric tumor, representing only 1% of all pediatric malignancies, with an incidence of approximately 1 per million. In this context, an urgent needing not yet addressed is the random assignment to adjuvant chemotherapy of high-risk stage II and stage III colon cancer patients, both young and adults, without any predictive factor of efficacy. Secondly, in the field of drug discovery the critical step is the preclinical evaluation of drug cytotoxicity, efficacy, and efficiency. We purpose to develop a patient-derived 3D preclinical model useful for drug evaluation that can mimic *in vitro* the patient's disease.

Methods: Surgically resected healthy colon mucosa and matched CRC were decellularized by a detergent-enzymatic treatment (DET). DET scaffolds were recellularized with HT29 cells. Qualitative and quantitative characterization of matched recellularized samples were evaluated through histology, immunofluorescences and DNA amount quantification. Chemosensitivity test was performed using increasing concentration of 5-Fluorouracil (5-FU), range 0.1 µM to 100 µM. *In vivo* studies were carried out using the zebrafish (*Danio rerio*) animal model. For cancer xenograft assays, HT29 cells were injected into the duct of Couvier and subsequently incubated in 96-well plates with different concentrations of 5-FU. Drug absorption and perfusion along fresh and DET tumor scaffolds were evaluated qualitative using autofluorescence of doxorubicin (doxo, 594nm) and quantitative calculated by Darcy’s law. Buffy coat-derived monocytes were cultured with DET scaffolds and macrophages

lineage markers were evaluated with flow cytometry.

Results: Decellularization protocol allowed the preservation of original structure and ultrastructure (SEM analysis). Five days after recellularization with HT29 cell line, the 3D CRC model exhibited reduced sensitivity to 5-FU treatments compared with conventional 2D culture. Calculated IC50 resulted in 11.5 µM and 1.3 µM of 5-FU, respectively. In the zebrafish transplantation model, HT29 extravasation was detected after 4 days post injection. Moreover, we obtained a 5-FU IC50 comparable with that observed in the 3D CRC model. Using confocal microscopy, we demonstrated that doxorubicin diffuses through the volume of 3D CRC model and co-localize with the cell nuclei which repopulate the 3D CRC scaffold. Finally, we observed that monocytes exposed to tumor decellularized ECM differentiated towards a pro-tumoral anti-inflammatory macrophage-like profile.

Conclusion: 3D CRC model could be preclinical reliable tool to bridge the gap between *in vitro*, *in vivo* and ex vivo drug testing assays. The 3D CRC model, translated in the pediatric setting, could help clinicians and oncologists to identify the most suitable treatment for the patient.

1.INTRODUCTION

1.1 Colorectal cancer in young and adult patients: epidemiology, classification and treatments

Colorectal cancer (CRC) is one of the most common malignancies in the world, third diagnosed cancer cause and second cancer cause of death globally, accounting for more than 1.8 millions estimated new diagnoses (crude rate 24.2 per 100,000 people) and more than 880,000 estimated deaths (11.5) in 2018 [1]. Given the temporal profiles and demographic projections, the global burden of CRC is expected to increase by 60% to reach more than 2.2 million new cases and 1.1 million cancer deaths by 2030 [2]. In contrast, CRC is a rare pediatric tumor, representing only 1% of all pediatric malignancies, with an incidence of approximately 1 per million [3-4]. CRC is a heterogeneous disease that originates from a multi-stage biological process characterized by progressive deregulation in the oncogene and oncosuppressor genes. Such genotype alterations are associated to phenotypic alterations characterized by the progressive de-differentiation of colic epithelial, the so-called “adenoma-carcinoma sequence” [5]. (Figure1)

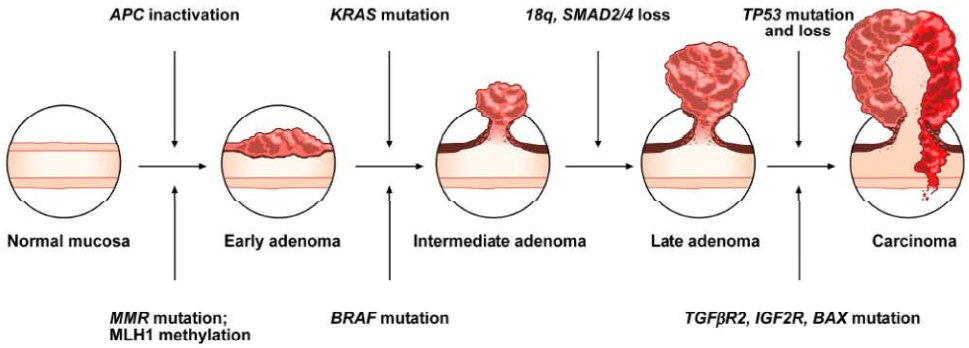

Figure 1: Anatomo-pathological evolution of the adenoma-carcinoma sequence [6].

Approximately 25% of CRCs in adults are hereditary [7]. Hereditary non-polyposis colorectal cancer (HNPCC) and familial adenomatous polyposis (FAP) are the most important cancer predisposition syndromes associated with CRC. HNPCC and FAP are inherited in an autosomal dominant fashion and account for approximately 2 and 0.1–1% of all adult cases of CRC, respectively. Other polyposis syndromes include the Peutz-Jeghers syndrome and juvenile polyposis coli [8].

FAP is generally caused by germline inactivating mutations in the adenomatous polyposis coli gene (APC). *APC* is a tumor suppressor gene and is a member of the WNT pathway located at 5q21 [9]. FAP is a dominantly inherited syndrome affecting 1 in 7,000 individuals with high penetrance; affected patients have a nearly 100% chance of developing CRC at an early age. Children with this mutation should undergo frequent colonoscopy screening from age 10 to age 14. Ideally, annual sigmoidoscopy should start by the age of 10, and prophylactic colectomy should be considered at age 15 or as soon as polyps are identified. Two clinical variants of FAP, which have the same risk of progression to CRC, and extra-intestinal tumors have been clinically identified. Gardner syndrome, one of the clinical variants of FAP, also presents with osteomas, desmoid tumors, epidermoid cysts, fibromas, and congenital hypertrophy of the retinal pigment epithelium. The other FAP variant, Turcot syndrome, involves multiple brain tumors (medulloblastoma, glioma, and ependymoma) and usually occurs in pediatric patients in conjunction with FAP [10].

Mutations on chromosome 1p33-34 involving the *MUTYH* gene (OMIM n. 608456) are associated with a relatively milder form of polyposis termed MUTYH-associated polyposis (MAP). These mutations may be present in 10–30% of patients without a mutation in *APC*; *MUTYH* mutations are important biomarkers that are useful for identifying FAP patients, especially those with an attenuated phenotype [11].

HNPCC, also known as Lynch syndrome, is an uncommon autosomal dominant hereditary condition. It is caused by a mutation in one of several DNA mismatch repair (MMR) genes: *MLH1*, *MSH2*, *MSH6*, or *PMS2*. Mutations in these genes lead to microsatellite instability (MSI).

The remaining 75% of CRC in adults is of sporadic origin. The acquisition of genetic instability as key event of tumor progression is to be attributed to three main genetic factors: 85% of sporadic CRCs exhibit chromosomal instability (CIN) in the form of structural or numerical anomalies of the chromosomes in the tumor cells. About 10% of sporadic CRCs are characterized by MSI, associated with the biallelic inactivation of genes involved in DNA repair. Finally, 5% of sporadic CRCs shows a characteristic epigenomic instability understood both as global hypomethylation and as an alteration in methylation of the CpG [12].

The most common CRC classification, considered valid for both young and adult patients, is the TNM classification system of the American Joint Committee on Cancer (AJCC). The TNM system has been in force around the world since the mid-1980s and is based on the evaluation of three parameters: parameter T (Tumor), indicates the degree of invasion of the intestinal wall; parameter N (Node), indicates the degree of involvement of locoregional lymph nodes; the parameter M (Metastasis), indicates the presence or absence of metastasis [13] (Table 1). Patients with CRC stage I, II and III have 5-year Disease-Specific Survival rates (DSS rates) of 95%, 84.7% and 68.7%, respectively, and 5-year Overall Survival rates (OS rates) of 82.7%, 70.3% and 58.3%, respectively. CRCs that have spread to other parts of the body are often harder to treat and tend to have a poorer outcome. Metastatic, or stage IV colon cancers, have a 5-year OS rate of about 11% [14].

AJCC stage	TNM classification	TNM stage criteria for colorectal cancer
Stage 0	Tis, N0, M0	Tis: Tumor confined to mucosa; cancer-*in-situ*
Stage I	T1, N0, M0 T2, N0, M0	T1: Tumor invades sub mucosa T2: Tumor invades muscularis propria
Stage IIA	T3, N0, M0	T3: Tumor invades subserosa or beyond (without other organs involved)
Stage IIB	T4a, N0, M0	T4a: Tumor penetrates to the surface of the visceral peritoneum
Stage IIC	T4b, N0, M0	T4b: Tumor directly invades or is adherent to other organs or structures
Stage IIIA	T1-2, N1, M0 T1, N2a, M0	N1: Metastasis to 1 to 3 regional lymph nodes.
Stage IIIB	T3-4a, N1, M0 T2-T3, N2a, M0 T1-T2, N2b, M0	N1: Metastasis to 1 to 3 regional lymph nodes.
Stage IIIC	T4a, N2, M0 T3-T4a, N2b, M0 T4b, N1-N2, M0	N2: Metastasis to 4 or more regional lymph nodes
Stage IV	any T, any N, M1a/b	M1: Distant metastases present; M1a: Metastasis confined to one organ or site; M1b: Metastases in more than one organ/site or the peritoneum

Table 1: TNM classification system of the AJCC, according to the "TNM Classification of Malignant Tumors.

Regarding the treatments, there are no prospective studies for CRC in young patients. The indication should follow treatment recommendations based on adult experience and considering the staging of the individual patient. Surgery is a key component of CRC treatment. In young patients with known polyposis syndromes, a tumor can be diagnosed earlier when it develops within a polyp, and these children can often be cured by polypectomy during colonoscopy. However, in most young patients, radical surgery is

necessary to obtain a radical resection of all tumor manifestations even if radical procedures such as wide or multivisceral resections and peritonectomy are needed.

The 5-year survival rate of children with early stage tumors (TNM stage T1–2, N0, M0) is over 90%, and in these cases, no adjuvant therapy is recommended after surgery. Two features facilitate the categorization of a patient with stage II CRC as a high-risk patient: a pT4 tumor and a low frequency of satellite instability (MSI-Low). However, in young patients, it may be important to categorize those with pT3 tumors, a high histological grade (3– 4 for MSI-High), perforation or occlusion, less than 12 lymph nodes studied, and undetermined or compromised surgical margins (and perhaps those where the margin is close) as high-risk patients. Determination of mismatch repair (MMR) is crucial because tumors that are MMR deficient have a better prognosis and are more sensitive to chemotherapy than MMR proficient tumors.

Adjuvant treatment modalities include chemotherapy, radiotherapy, and more recently, biological targeted therapy. Postoperative radiotherapy has been typically used for rectal cancer in combination with 5-Fluorouracil (5-FU) based chemotherapy. However, recent experience in pre-operative radiotherapy for advanced adult cases might suggest a role for this therapy in decreasing the risk of recurrence following surgery, or occasionally to allow for a less invasive surgical procedure [15]. The use of radiotherapy for CRC is complicated by the occurrence of radiation-induced enteritis and is limited by the difficulties in targeting the tumor volume. Treatment of node-negative patients at stage T3–4 is controversial. New reagents such as capecitabine, oxaliplatin, irinotecan, cetuximab, or bevacizumab have proven to be active in advanced disease and are now under evaluation in the adjuvant setting [16-18]. For patients with resected CRC with lymph node involvement (stage III), adjuvant chemotherapy based on 5-FU/folinic acid (5FU/FA) is recommended [19]. Globally, it can be said that even today 5-FU represents

the cornerstone of CRC treatments both in young and adults patients [20-21]. Particular attention have to go to patients with high-risk stage II and stage III colon cancer: surgery is a curative treatment for these patients, but 40 to 50% who undergo the surgery alone, ultimately relapse and die of metastatic disease. In this context, it is important to known that these patients were randomly assigned to receive an adjuvant treatment in order to reduce recurrence and metastasis formation. FOLFOX adjuvant chemotherapy made up of the drugs FOL– Folinic acid (Leucovorin), F – Fluorouracil (5-FU), OX – Oxaliplatin (Eloxatin) has been shown to improve recurrence-free survival and overall survival both in children and adults by more than 20% and is nowadays considered a standard of care. However, the vast majority of patients will not benefit from receiving adjuvant chemotherapy because they have already been healed by the surgery or because of the development of drug resistance [22].

1.2 The Italian TREP project

Over the past decades, considerable progress has been made in the management of CRC in adults, leading to a significant improvement of overall survival. This has been attributed in part to aggressive surgical approaches and in part to our understanding of the disease's molecular biology and emergence of newer molecular targets [23]. Such an improvement in survival has not been seen in pediatric age. The rare cases occurring in children and adolescents characteristically carry a poor prognosis, related mainly to late diagnosis and advanced stage at presentation, but also to biological aggressiveness (i.e., high-grade disease and poorly differentiated, signet ring or mucinous adenocarcinoma histologies with a higher incidence of microsatellite instability) [24].

To offer clinical support for physicians encountering such uncommon cases, the Rare Tumors in Pediatric Age (TREP, Tumori Rari in Età Pediatrica) project was set up in 2000 in Italy with the purpose of collecting epidemiological data and developing diagnostic and therapeutic guidelines for the management of rare pediatric tumors (i.e., pediatric solid malignancies with an annual incidence <2 million), so that pediatric oncologists and surgeons can cooperate with experts in adult oncology in the management of such "orphan" diseases [25]. In the context of gastrointestinal tract carcinoma, it reports guidelines about clinical features, treatment, and outcome based on fifteen patients registered in Italy over the years 2000–2016. Most of the tumors were colorectal carcinomas (12/15 cases). Over the years, TREP has started new partnerships with associations such as EXPeRT (The European Cooperative Study Group for Pediatric Rare Tumors) to become more and more competent and cohesive in drafting guidelines in the field of rare pediatric tumors. EXPeRT was founded in 2008 by national groups from Italy, France, United Kingdom, Poland and Germany with the aim to perform initiatives including international data exchange, retrospective and prospective studies of specific entities, and the development of harmonized and internationally recognized guidelines. [26]

With the present work we hope to set a model that, translated in the pediatric setting, and in particular for gastrointestinal tract carcinoma, could help clinicians and oncologists to identify the most suitable treatment for the pediatric and young patients.

1.3 Preclinical CRC models: from conventional culture to three-dimensional culture system

1.3.1 Conventional two-dimensional culture system

The best experimental approach to develop an effective anticancer therapy is to comprehensively understand the mechanisms responsible for the onset, the development and the tumor diffusion. However, in such a complicated microenvironment it is difficult to understand, with current technologies, the key role of biological, biochemical, biomechanical, and biophysical factors that might drive human pathophysiology in a omni-comprehensive model. A possible approach against this challenge is the deconstruction of the complex cellular microenvironment into a simpler and more predictable system. In this scenario, the development of anticancer therapies has traditionally relied on two-dimensional (2D) cultures [27]: much of what we know about cancer and many successes in drug development derive from the use of this experimental model. In the two-dimensional setting, cells grown flat and adherent as monocultures on functionalized plastic culture plates [28]. The main advantages of this model are: a) cells grow easily and are easy to maintain [28]; b) cells are pure and free from other contaminating cells [28]; c) the manipulation of cells such as induction/silencing of genes and proteins, stimulation with biological factor and/or chemo-radiotherapeutic treatment are relatively easy [28]; d) the methods for the cytotoxicity evaluation of administered molecules are simple, highly standardized and reproducible [28], and e) the methods of protein/RNA/DNA extraction are relatively simple [28]. However, adherent cultured cells show clear limitations that have encouraged the development of more realistic and reliable models, such as the 3D culture systems.

As a matter of fact, it is now well accepted that monolayer cells do not grow in a physiological environment that allows them to assume the different shapes and behaviors

observed *in vivo*. In 2D cultures, cells are forced to polarize and increase their exchange area to culture media due to the attachment to rigid and flat substrates [29]. This leads to an over-nutrition, over-oxygenation and non-reproducibility of the *in vivo* molecular gradients. In addition, in the 2D setting, the composition, configuration and production of extracellular matrix (ECM) are significantly altered [18]. This poses a relevant limitation in using 2D cell cultures for drug testing: anti-cancer agents administered to 2D cell cultures reach cells without any physical barrier leading to an over exposition of cells [30],while the same molecules delivered *in vivo* encounter a different associated stroma, different cell–cell contacts and cell–matrix interactions that significantly affect drug's concentration throughout the tumor microenvironment [30]. Finally, even more evident in the anticancer treatments is the fact that cells can behave differently depending on their environment and culture conditions: medium supplements, cell density, and composition of the culture surface have a critical impact on cell proliferation, differentiation, migration, and death by affecting intracellular signal transduction and leading to unpredictable reactions to exogenous stimuli [31]. Undoubtedly, immortalized 2D cancer cells have contributed greatly to the knowledge about tumor biology, signaling pathways, and the investigation of new substances. However, this model fails to represent the real complex tumor architecture. It was estimated that only 5% of active drugs in cellular models were found to be active in clinical trials [32]. This reason brought researchers to develop more sophisticated *in vitro* approaches, i.e., 3D models, which recapitulate certain features of solid tumor tissues, such as tumor morphology, gradient distribution of chemicals and biological factors, and reciprocal interactions/constraints between tumor and its stroma.

Culture technique	Surface/ Materials	Advantages	Disadvantages
Undiferrentiated flat cell monolayer	Plastic surface (culture dishes or flasks)	Cells grow easily and are easy to maintain, cells are pure and free from other contaminating cells, treatment are relatively easy; the methods for the cytotoxicity evaluation of a molecule are simple, highly standardized and repeatable, the methods of protein/RNA/DNA extraction are relatively simple	Undifferentiated cells without any tissue-specific organization, adhesion of cells to stiff affects gene expression and drug response; no cell-cell interaction, no cell-ECM interaction
Scaffold-free 3D culture system	Spheroids, tumoroids, organoids, colospheres - liquid overlay culture medium, any artificial cell adhesion substrate	Spheroids skills gradients of oxygen, nutrient and metabolism; moreover closely resembled ultrastructure and organization of the same cells when grown as tumors *in vivo.* After treatment with drugs spheroids exhibit resistance, comparable to the *in vivo* situation	Cell number is limited, low stability difficult long-term culture
Scaffold-based 3D culture system	Synthetic scaffolds PVDF, Macroporus Hydrogel	Biocompatible, biodegradable and reproducible matrix composition	Generate an artificial barrier between the tissue and the surrounding environment; require chemical functionalization (RGD) to allow cell adhesion. Residual synthetic compounds may have cytotoxic effects
	Natural scaffolds-animal derived matrices-collagen Gel, Matrigel, silk protein	Flexible physiologic matrix-environment allows 3D growth on natural ECM components	Matrigel when polymerized, is not suitable for long-term storage of samples, because it can dissolve, especially if stored cooled. Matrigel gel forms a dense structure that forms a diffusion barrier which can interfere in some biochemical and toxicological assays in addition, it contains residual heparan sulfate growth factors, lacks human motifs, and contains undefined substances that make difficult the comparison and analysis of results cause of batch-to-batch variation
	Natural scaffolds-plant derived matrices-methylcellulose, agarose and alginate	Cells encapsulated in alginate are able to proliferate in 3D-colonospheres	Batch variability and lack reproducibility

Table 2: Summary of the difference between 2D and 3D culturing platforms.

1.3.2 Scaffold-free 3D culture systems

According to their composition, 3D culture systems can be divided as scaffold-free or scaffold-based (of natural or synthetic origin) methods.

In oncological research, the addition of the third dimension to cell culture dates back to the '70s with the seminal experiment of Sutherland and coworkers. After cultivating Chinese hamster V79 lung cells in suspension culture, they obtained spheroids morphologically resembling mammary carcinoma nodules Soranzo and Ingrosso (1986), after growing LoVo human colon carcinoma cells by using the liquid overlay technique, successfully cultivated what they defined the multicellular tumor spheroids. Initially, they observed that growth kinetics were different if compared to monolayer culture: doubling times were found to be 5 days and 37 h for LoVo spheroids and monolayer cells, respectively. In addition, they observed that cell ultrastructure and organization in spheroids closely resembled those of the same cells when grown as tumors *in vivo*. Surprisingly, they found that three out of five molecules were less cytotoxic on spheroids than on monolayer cells in both growth conditions [33]. This result indicated that the different pattern of activity of these anthracyclines on a spheroid system is not only related to the presence of cells at different cell cycle phases, but depends also on the 3D ultrastructure, which significantly modifies drug penetration inside tumor microenvironment [33]. Since the beginning of the long history of 3D culture, it was clear that this system could give also important information about the relationship between tumor cells and infiltrating host cells, such as fibroblast, macrophages and lymphocyte. In 1981, Lees and colleagues generated a multicellular tumor spheroids model of HT29 colon cancer cells, grown *in vitro* and subsequently implanted in the peritoneal cavity of BALB/c mice. The spheroids were recovered at various time and, after dissociation,

assessed for the viability by using a clonogenic assay. During the initial four days after implantation, only a little damage was observed to spheroids, but more than 99% reduction in clonogenic tumor cells occurred between days four and seven [34]. Coupled to the functional test of clonogenic assay, the morphological test (light and electron microscopy both in situ on sections and on dissociated suspensions of spheroid cells), demonstrated a correlation between spheroids damage and graft in situ destruction with host cell infiltration. Another important application of 3D culture was proposed by Sutherland et al. in 1989. Following to a first experimental approach, using hamster cells, they utilized LS174T human colon adenocarcinoma multicellular spheroids to study the radiobiological aspects of radioimmunotherapy [35]. In particular, the LS147T spheroids were incubated with an anti-CEA antibody labeled with I131, an instable ß-emitter radioisotope of iodine. The principal aims of the study were to accurately determine the absorbed doses and their biological effects. The results clearly showed that despite spheroid diameter was not significantly affected by the therapy, histological examination revealed a significant reduction in cell density, particularly in the area close to the spheroid surface [35]. Based on the fact that a positive response to chemotherapy implies a regression of tumor mass, Jansen et colleagues decided to exploit the potential role of spheroids in providing a complex 3D ultrastructural organization in order to investigate the ability of glycineamide ribonucleotide transformylase inhibitors to produce tumor regression in several preclinical models of colon carcinoma [36]. Tumor spheroid of WiDr human colon carcinoma were treated with a large series of GAR TFase inhibitors: some of them caused a growth inhibition of WiDr spheroids without showing any sign of regression, while other compounds showed a complete spheroid disruption [33]. The studies were then extended *in vivo* to assess the potential of those compounds that caused only growth restriction against those that caused tumor mass regression [36].

Interestingly, only those compounds that in the spheroids studies showed tumor mass regression produced an effective cure in animal model studies.

A study of Mueller-Klieser and colleagues (2002) investigating the effects of green tea extracts (GTE) on CRC cell viability and proliferation was based on the multicellular spheroids derived from WiDr [37]. In this study, they treated monolayer cells and spheroids with increasing concentration of GTE, demonstrating that whereas 20 µg GTE/mL did not induce significant changes in WiDr spheroids, the plating efficiency of WiDr monolayer cells was reduced by 40% of the control value (non-treated cells) at this GTE concentration. In addition, exposure to 100 µg GTE/mL was associated with a great decrease in monolayer cell plating efficiency, whereas changes in volume, growth and cell proliferation in spheroids were significant but relatively moderate.

At this concentration, GTE showed a strong cytotoxicity in WiDr monolayer cells while the spheroids showed only a moderate growth retardation and G2/M arrest [37]. The model of multicellular tumor spheroids was used by Mellor and colleagues (2005) to address the clinical relevant problem of the heterogeneous population of cells in solid tumors, in which the small proportion of actively dividing cells co-exist with a large number of quiescent cells [38]. The quiescent cell population of tumor limits the success of many anticancer therapies, because conventionally used chemotherapeutic agents target only proliferating cells [38]. On this basis, they developed a multicellular tumor spheroids model using DLD-1 human colon adenocarcinoma cells supplemented with classical complete medium called tumour spheroids proliferating (high expression of Ki-67 marker) and a quiescent version cultivated in serum-starvation setup, called tumour spheroids quiescent (high expression of quiescence marker p27kip1) [38]. Afterwards, the efficacy of widely used chemotherapeutic drugs was tested. Vinblastine, doxorubicin, cisplatin and 5-FU produced significant cell death in the TS proliferation. However, while

still effective, the potencies of doxorubicin and cisplatin were significantly reduced in TS quiescent status. Interestingly, 5-FU and vinblastine did not produce cell death in the TS quiescent status, thus indicating that within an *in vivo* tumor micro-regions subsist with cells that have different sensitivity to chemotherapy due to a complex ultra-structural organization. A similar result was observed by Mohanty et al. in which the potential of multicellular spheroids derived from HCT-116 colon carcinoma cells represented an high throughput screening tools to evaluate the potential of a chemical library of compounds capable of reducing viability and inducing apoptosis [39]. Using this model, they identified NSC647889 as a potent apoptotic novel compound, able to dramatically increase tumor cell apoptosis in multicellular spheroids compared to standard antineoplastic agents [39]. However, they observed a fraction of quiescent cells, located in spheroid cores that were resistant to NSC647889-induced apoptosis. These data suggest that cells in hypoxic and nutrient limited areas are resistant to apoptosis and die for other mechanisms [39].

Models able to creating an *in vitro* cellular culture better recapitulate complex tissue architecture and mechanical stimuli, the multicellular tumor spheroid culture system was recently coupled with the technology of microfluidic systems integrated in bioreactors. In this scenario, Chen and colleagues (2015) developed a micro-engineered platform fabricated from polydimethylsiloxane (PDMS) using soft lithography and rapid phototyping, highly effective in generating homogenous and large numbers of tumor spheroids with in addition the advantages of body fluid flow simulation [40]. Other advantages are the capability of generating tumor spheroids with uniform structure, possibility of long-term cultivation, and real-time imaging measurement [40]. Using this tool, they performed cytotoxicity tests for doxorubicin and paclitaxel using multicellular tumor spheroids derived from HCT-116 and the same cells cultivated in monolayer.

Consistently with the previous findings using other *in vitro* 3D cancer tissue models, the apoptotic rate after treatment decreased by 26% on the multicellular tumor spheroids compared to 2D cultures [40]. Interestingly, they clearly demonstrated a negative correlation between cell-cell contact and drug susceptibility. In fact, by increasing the tumor spheroid size, the sensitivity to doxorubicin, and similarly to paclitaxel, decreases [40].

1.3.3 Scaffold-based 3D culture systems

1.3.3.A Biomaterials in tissue engineering

Nowadays, there has been a huge progress in the development of biomaterials to support scaffold formation both for drug screening and regenerative tissue. The birth of tissue engineering and, at the same time, the birth of biomaterials occurred in the early 1990s. A biomaterial is defined as any substance that has been engineered to interact with biological systems for medical, therapeutic or diagnostic purposes [41]. A fundamental characteristic of biomaterials is biocompatibility, defined in 1986 during Consensus Development Conference, as the ability of a material to act by determining an appropriate host response to a given application. In the last decade, special attention has been paid to the development of 3D scaffolds. Scaffolds, which are generally polymeric materials, are designed to allow a better adhesion, growth, differentiation and diffusion of cell in relation of 2D. In particular, for the evaluation of a new drug it is necessary to use a porous scaffold compatible with biofactors, such as the cells that will be used for its repopulation [42]. A decisive factor in determining the success of the model is the correct design of the scaffold. The scaffold aims to replace the ECM, thus influencing the biomechanical, biochemical, and biological properties of tissues and cells. In particular, it

must meet the following two requirements: a) a degree of porosity enable to constitute a percolating pattern that favors cellular growth and disposition, nutrient intake, and disposal of metabolic products [43], and b) an appropriate surface characterized by adequate physical-chemical properties (topography, surface charge, adsorption and protein release) [44], in order to promote adhesion, growth, proliferation, differentiation, and migration of cells [45]. There are several studies that employ methods based on scaffolds, either of natural or synthetic origin, to build 3D tumor models to be used for drug screening.

1.3.3.B Synthetic scaffolds

Synthetic scaffolds, inevitably induce an immune response and, since they often show a reduced interaction with cells and biological environments, generally stimulate a poor cellular response [46]. The most common synthetic polymers used to build 3D tumor models include linear polyesthers, polylactic acid (PLA), polyglycolic acid (PGA), polyvinylidine fluoride (PVDF), polylactic-co-glycolide (PLGA) [47] copolymer and polycaprolactone (PCL) [48]. Casciari and colleagues utilized the synthetic polymer polivinilidenfluoruro, PVDF, to test doxorubicin in human colon cancer cells SW620 [49]. Doxorubicin toxicity, expressed as lethal concentration (LC50), was found to be 3.5 mM in the PVDF 3D fiber culture versus 0.16 mM found in the monolayer culture. The 3D synthetic model showed a significantly higher drug resistance. Despite their biocompatibility, the presence of PVDF fibers generate an artificial barrier between the pathological tissue and the surrounding environment, this contact limitation ends up excluding the flow of large molecules such as antibodies [49]. Thus, due to the presence of this barrier, this model should not be considered for studies of drug delivery with nanoparticles that would not be able to penetrate.

An important factor to consider for the design of a scaffold is represented by the compatibility between cells and the scaffold itself. Generally, cells have no receptors to adhere to synthetic scaffolds [50]. An increased adhesion can be achieved by superficial modification of the scaffolds in order to allow better cell adhesion and penetration. In this scenario, modification of the scaffolds whit Arg–Gly–Asp (RGD) peptides, which represent the natural binding site for a subset of integrins to ECM proteins, including fibronectin, laminin, vitronectin, and collagen has been developed [50].

1.3.3.C Natural scaffolds

Natural scaffolds are constituted by natural polymers derived from animals or plants [51]. The most commonly used animal-derived polymers are collagen, fibrin, glycosaminoglycan, and hyaluronic acid. Among them, gel systems, such as collagen-based scaffolds, represent one of the earliest biomaterials and are still used nowadays since collagen is one of the most abundant components of the ECM. Collagen gel consists of macromolecular hydrophilic cross-linked polymers [52]. Tarig Magdeldin et al. developed an *in vitro* 3D tumor model based on the removal of interstitial fluid from collagen hydrogels whit the aim to create a multiwell drug testing platform [53]. In details, an absorber was put on the hydrogel for 15 minutes and the consequent removal of some fluid led to the concentration of cells and collagen to physiological conditions. In this 3D platform the anti-epidermal growth factor receptor (EGFR) chemotherapeutic agent Cetuximab was tested in the two CRC cell lines HT29 and HCT-116 (KRAS mutant and KRAS wild-type, respectively) both in 3D and 2D cultures [53]. Gene expression levels of EGFR, measured with one-step quantitative reverse transcription polymerase chain reaction (qRT-PCR), revealed a two-fold and three-fold increase in 3D cultures for both HT29 and HCT-116 cells, respectively, compared to the monolayer

(used as controls). Furthermore, in agreement with their KRAS mutant status, HCT-116 cells both in 2D and in 3D, were non-responsive to drug whereas Cetuximab levels were significantly lower in HT29 3D cultures in comparison to 2D ones [53]. Matrigel is another largely used hydrogel [54]. It consists of a basal membrane preparation in a solution extracted from Engelbreth-Holm-Swarm (EHS) mouse sarcoma, a tumor rich in ECM proteins. The main components are: laminin, collagen IV, entactin, and proteoglycan eparan-sulfate [55]. The extract also contains growth factors, naturally present in EHS sarcoma. At room temperature, Matrigel polymerizes to produce a biologically active matrix that represents the basal membrane of mammalian cells [55]. Matrigel can be used as a coating of porous filters as a barrier to test tumor cell invasion capability in Matrigel chambers. Recently, Dorward and colleagues studied the role of Aquaporins (AQP) in tumor progression [56]. In particular, they found a different expression of AQP1 in HT29 and HCT-116 cell lines (high and low AQP1 levels, respectively) after adding the AQP1 inhibitor AqB013 [56]. With the use of a Matrigel chamber, they demonstrated a correlation between AQP1 activity and colon cancer cell migration and invasion [56]. At clinical level, the inhibition of AQP1 may slow the progression of CRC and increase the intervention window, especially in early stage cases. One limitation of Matrigel is that, once polymerized, the matrix is not suitable for long-term storage because it can dissolve [57]. The gel forms a dense structure that can interfere with some biochemical and toxicological dosages [57]. Sometimes Matrigel contains residuals of heparan sulfate growth factors, lacks human motifs, and contains undefined substances that make difficult the comparison and analysis of results because of batch-to-batch variation [58].

An innovative 3D model of intestine, proposed by Kaplan and his group [59], belongs to the animal scaffold category [60] .This group developed a 3D porous scaffold system,

using silk proteins to mimic both the structure and function of native intestine [59]. Kaplan's 3D geometrically-engineered hollow lumen provided a monolayer of epithelial cells, surrounded by myofibroblasts dispersed in the porous scaffold bulk. The innovative characteristics of the model are the ability of maintaining a continuous mucus double layer and to present a proximal-to-distal reduction in oxygen tension through the intestinal lumen. Co-cultures cells on 3D scaffolds were maintained for 8 weeks and higher level of intestinal markers where maintained during all time long. This system was proposed for studying drugs absorption and for microbiota evaluation [59].

On the other hand, the most used plant-derived polymers are methylcellulose, agarose and alginate [61]. Alginate is a natural non-toxic anionic polysaccharide, and is well known in literature for its modulastion with cell proliferation, survival, production of ECM compounds and tumor invasion [62-64]. Buhrmann *et al.* investigated an alginate-based 3D scaffold for the screening of 5-FU alone or in combination with curcumin in HCT-116 cells and in the corresponding isogenic 5-FU-chemoresistant cells (HCT-116R). CRC cells encapsulated in alginate were able to proliferate in 3D-colonospheres for over 21 days and showed an *in vivo*-like phenotype not visible in 2D. During cultivation of cells in alginate. They have been able to observe three different cell states of (1) proliferation, (2) invasion, and (3) adhesion [65]. By performing western blot analysis and quantitative densitometry, they evaluated the tumor-promoting factors CXCR4, MMP-9 and NF-κB and demonstrated an increased proliferation and invasiveness in the 3D model compared to the adherent cells They also observed that HCT-116R cells overexpressed tumor-promoting factors in comparison to the parental HCT-116 [65]. In the alginate 3D scaffold, curcumin in combination whit 5-FU induced a decreased capacity in proliferation and invasion and increased the sensitivity to 5-FU of HCT-116R cells compared to the HCT-116 cells. 5-FU half maximal inhibitory concentration (IC50) for

HCT-116 was 8nM, but it was found to be significantly reduced when co-administered with curcumin [65]. This was the first study to describe a 3D biocompatible microenvironment for the long-term cultivation of CRC cells leading to an improvement in the quality of *in vitro* drug screening in a pre-testing animal-free model [65].

1.3.3.D 3D bioprinting

Bioprinting is defined as the synchronous positioning of biomaterials and living cells in a prescribed layer-by-layer stacking organization to fabricate 3D constructs [66]. Three-dimensional printing promises even greater utility if correlated with tissue engineering, by potentially allowing pharmaceutical applications such as targeted drug delivery and 3D organs for transplantation [67], drug efficacy or toxicity studies [68]. Bioprinting can be performed in two different ways, namely (1) scaffold-based and (2) scaffold-free bioprinting [69]. The first option provides cells bioprinted within exogenous biomaterial matrix [69] while, in the latter, cells are printed with an inert gel support, which offers the initial structural stability that later, after maturation, is discarded. The most suitable bioprinting model should be selected on the basis of the type of pharmaceutical studies (drug discovery/drug development/drug delivery etc). Scaffold-free bioprinting has become increasingly relevant in anti-cancer drugs research because cells can grow in a manner more similar to the one observed *in vivo*, for example the presence/formation of the hypoxic cores which influence drug response [70]. There are three main types of bioprinting modalities, *i.e.*, droplet-based bioprinting (DBB), extrusion-based bioprinting (EBB), and laser-based bioprinting, which have been described in detail by Peng and colleagues [71]. So far, several bioprinted tissues with different cells types and scaffolds have been fabricated as *in vitro* models for testing drug efficacy, toxicity, chemotherapy

and chemoresistance [71]. To date, there are no published data on 3D bioprinted intestine models for drug testing, probably due to it complex structure and functions (such as absorption and secretion). Nevertheless, only very few constructs have been commercialized, an example is the liver tissue model exVive3D, employed to screen liver toxicity of drugs [72].

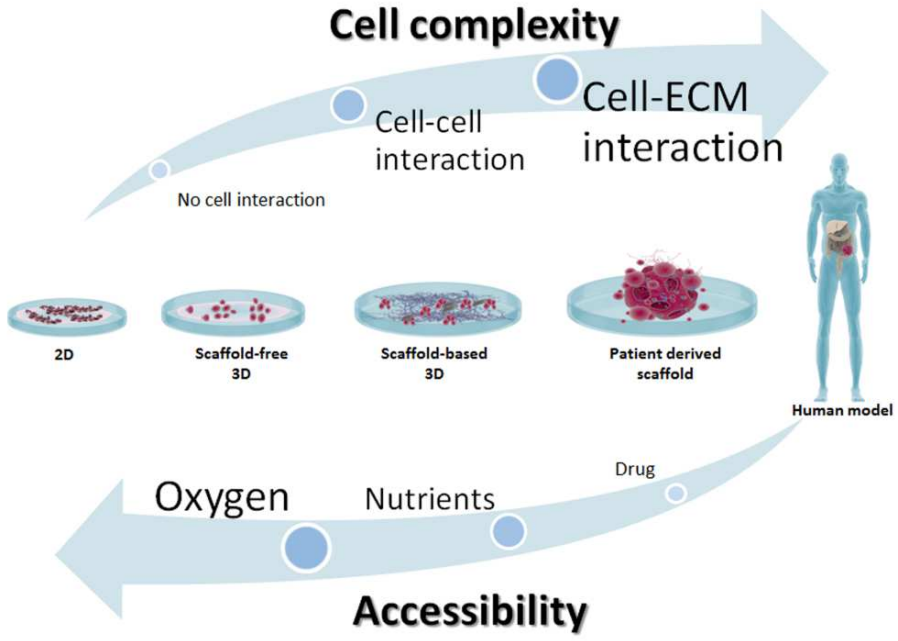

Figure 2: Conceptual progression from *in vitro* 2D cell model to human model. 3D tumor models show many advantages over 2D, such as microenvironment parameters and cell−ECM interactions [73].

1.4 Tissue engineering applied to oncology: the decellularization and ricellularization process

The term decellularization means the removal of the cellular component of a tissue by minimally altering its biochemical composition and its biological and structural properties. Currently, there is no precise quantitative or qualitative requirements that allow to uniquely defining the yield of tissue decellularization. Nevertheless, the following minimal criteria

identified in literature are considered sufficient to satisfy the intent of decellularization [74]:

• <50 ng dsDNA per mg of dry weight ECM;

• <200 bp DNA fragment length of the remaining DNA;

• lack of visible nuclear material in tissue sections stained with 4',6-diamidino-2-phenylindole (DAPI) or Hematoxylin and Eosin (HE) stain.

Several decellularization techniques can be employed, depending on the characteristics of the tissue, as size, cellularity, density and thickness [75]. Figure 3 summarizes some of the most common decellularization approaches, that can be divided in three categories: physical, enzymatic or chemical treatments. These techniques can be used individually or in combination in order to disrupt cell membranes, release cell contents and degrade nuclear material, without damaging the tissue ultrastructure [76].

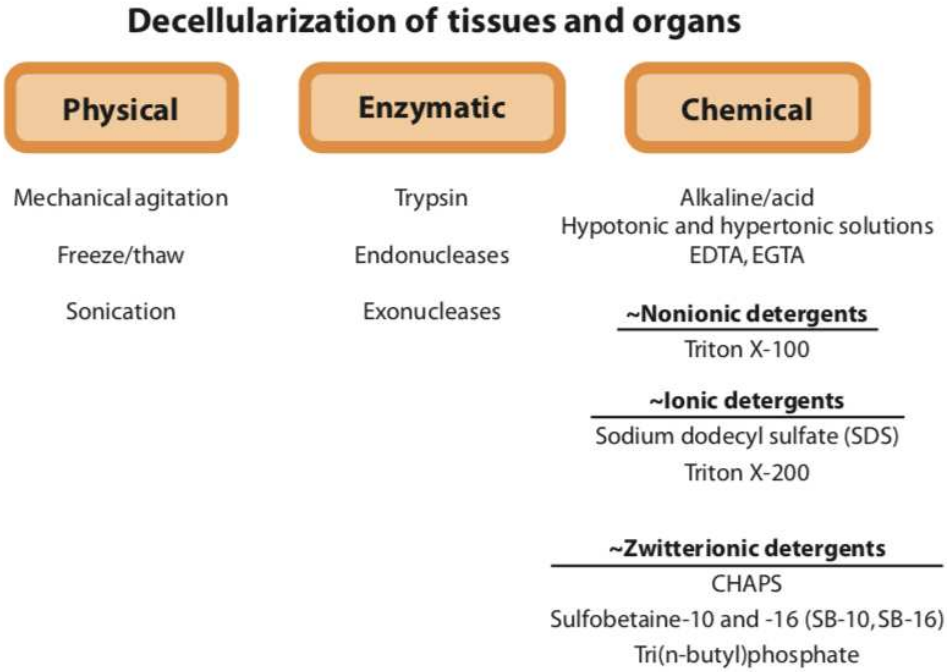

Figure 3: Examples of decellularization techniques [76].

Organs such as heart [77], lung [78], liver [79] and oesophagus [80] have been successfully decellularized and recellularized, constituting a promising solution for both drug evaluation and replacement of organ failure. Undoubtedly, the principal advantage of using biological-derived matrices instead of synthetic polymers for *in vitro* 3D tumor study is that a portion of the main structural proteins and soluble factors are already present in the decellularized scaffolds, allowing for a more physiological tissue reconstruction [81]. For this reason, decellularization has recently been applied in an attempt to unravel the complex and fundamental role of ECM in tumor progression, inflammation and metastasis. Different studies on CRC demonstrated that ECM components accumulating in the surrounding tumor area can be responsible of either containment of tumor growth or tumor progression with a poor prognosis, suggesting a complex and crucial role of ECM on cancer progression [82]. Until now, 3D intestine scaffolds have been developed as platforms for *in vitro* studies of cancer cell growth, survival, proliferation, migration and invasion [83]. Recently, Chen and colleagues created a physiologically active ex vivo model by decellularizing normal human colon tissue under conditions that preserved ECM and then reseeding primary colonic epithelial cells, endothelial cells and myofibroblasts [81]. They used this model to study CRC progression and to discover cancer-initiating and cancer-related genes [84]. So far, decellularization protocols present in literature relies on long incubation times [84]. Recently, our lab developed a new approach for the realization of patient-derived 3D matrices using a technique that provides short incubation time for the decellularization of healthy colon mucosa and CRC biopsies derived from the same patient undergoing surgery [85].

2.PURPOSE OF THE THESIS

The PhD project had the final goal to develop an *in vitro* patient-derived 3D model of colorectal cancer that mimics the patient's disease to be used as a laboratory tool to study both the adult pathology and, although rare, the pediatric one.

In particular the PhD project that I carried out during these three years had the following aims:

a) To standardize and characterize a decellularization and recellularization protocol for the healthy colonic ECM and CRC counterpart able to maintain native structural microenvironment and to sustain cell survival and proliferation;

b) To compare chemoresponse in conventional 2D cultures, a 3D patient-derived model and *in vivo* model in order to establish a pre-clinical tool for anticancer drug screening assay;

c) To verify the permeability of the 3D model to understand diffusion pattern of the drug

3.MATHERIAL AND METHODS

3.1 Patients

A series of 23 paired normal mucosa (N) and cancer lesion (T) from CRC patients who underwent curative surgery were collected from First Surgery clinic, University of Padua (Department of Surgery, Oncology and Gastroenterology). All of the patients enrolled fulfilled the following criteria: histologically confirmed primary adenocarcinoma of the colon, age > 18 years and written informed consent (n. prot. 448/2002). Patients with a known history of a hereditary colorectal cancer syndrome and which underwent neoadjuvant treatments were exclude

Age	media	67.73
	interval	39-83
Sex	male	15 (65.2%)
	female	8 (34.5%)
Grading	G1	2 (8.7%)
	G2	16 (69.6%)
	G3	5 (21.8%)
Staging (p-TNM)	I	1 (4.3%)
	II	6 (26%)
	III	10 (43.4%)
	IV	6 (26%)
Type of surgery	sigmoidectomy	9 (39.1%)
	hemicolectomy dx	9 (39.1%)
	hemicolectomy sx	5 (21.8%)

Table 3: Clinical and pathological characteristics of 23 patients enrolled in the study

3.2 Tissue decellularization

All mucosa specimens encompassed the luminal surface, mucosa and submucosa. CRC tissue was obtained at the edge of infiltrating neoplasia; healthy colon mucosa was obtained more than 10 cm far from the CRC. Surgically obtained N and T tissues were kept in cold and sterile phosphate buffered saline (PBS) for no longer than 2 hours before processing. All the steps of decellularization were performed with sterile solutions and under tissue culture hood. N and T tissues destined to be used as fresh were rinsed with sterile PBS and consequently treated according to the methodology with which were analyzed. Healthy mucosa and CRC destined to decellularization process were treated with two detergent-enzymatic treatment (DET) cycles. Each DET cycle was composed of deionized water at 4°C for 24 hours (h), 4% sodium deoxycholate (SDC) (Sigma) at room temperature (RT) for 4 h, and 2000 kU DNase-I (Sigma) in 1 M NaCl (Sigma) at RT for 3 h, after washing in water. After decellularization, matrices were rinsed in 3 % penicillin/streptomycin (pen/strep)/PBS for at least 4 days and then preserved at -80°C.

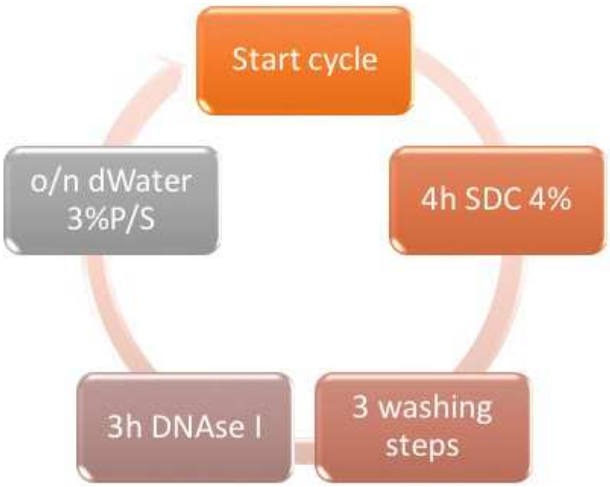

Figure 4: Schematical representation of DET cycles.

3.3 DNA isolation and quantification

To assess the total DNA content within the fresh N and T tissues, the recellularized three-dimensional normal tissues (3DN), the recellularized three-dimensional tumor tissues (3DT) and the corresponding decellularized matrices, each specimen was treated using the DNeasy Blood&Tissue kit (Qiagen) under manufacturer's instruction. The DNA samples were then quantified using Nanodrop 2000 spectrophotometer at the 260/280 nm ratio (Thermo Scientific, USA).

3.4 Immunohistochemistry and immunofluorescence

Frozen sections (8 µm thick) were stained with Haematoxylin & Eosin (HE; Bio Optica, Milan, Italy), Masson trichrome (aniline blue kit; Bio Optica), Periodic Acid Schiff (PAS; Bio Optica), anti-Collagen IV (1:100, Dako, Milan, Italy), and anti-MIB1 antibody (1:50, Dako, Milan, Italy). All the stainings were performed according to manufacturer's instruction. Immunohistochemical (IHC) stainings were automatically performed using the Bond Polymer Refine Detection kit (Leica Biosystems, Newcastle upon Tyne, UK) in the BOND-MAX system (Leica Biosystems). For immunofluorescence (IF) analysis, the sections were permealised with 0.5 % Triton X-100, blocked with 10 % horse serum and incubated with the primary antibodies Laminin (1:100, L-9393 Sigma); Ki-67 (1:100, ab15580 Abcam); E-cadherin (1:250, BD Biosciences) and Vimentin (1:100 ab92547 Abcam), TUNEL and EdU (Thermo Fisher Scientific). Slides were then washed and incubated with the labelled Alexa Fluor secondary antibodies diluited 1:200. Finally, nuclei were counterstained with fluorescent mounting medium (Sigma-Aldrich)

containing 100 ng/mL DAPI (Sigma-Aldrich). For each specimen, random pictures were collected with a direct microscope.

Antibody	Dilution	Manufacturer
Ki-67 (Rabbit)	1:100	Abcam
Vimentin (Mouse)	1:100	Abcam
Laminin (Rabbit)	1:100	Sigma-Aldrich
E-cadherin (Rabbit)	1:250	BD Biosciences
Collagen IV (Rabbit)	1:100	Dako
MIB-1 (Rabbit)	1:50	Dako
Anti-Rabbit 594	1:200	Thermo Fisher Scientific
Anti-Rabbit 488	1:200	Thermo Fisher Scientific
Anti-Mouse 594	1:200	Thermo Fisher Scientific
Anti-Mouse 488	1:200	Thermo Fisher Scientific

Table 4: Antibodies used in the study for IF and ICH.

3.5 Recellularization of the scaffolds

Normal and tumor decellularized matrices were incubated overnight with growth medium containing Primocin antibiotic (InvivoGen) at 4 °C. In order to normalize the intra-sample variability, scaffolds were cut into comparable dimensions (0,5 cm^2) before seeding. All matrices were then injected with $2.5x10^5$ HT29 cells, resuspended in 10 µL of Collagen I (diluted 2:3 with RPMI-1640), using a 30G syringe needle. Samples were incubated for 6 h in humidified incubator at 37 °C and 5 % CO2. Complete medium was carefully added

and changed every day. Recellularized samples were either formalin fixed and paraffin embedded for the IHC stainings or fixed in 4 % PFA and then included in OCT (optimal cutting temperature compound) for the immunofluorescence analysis.

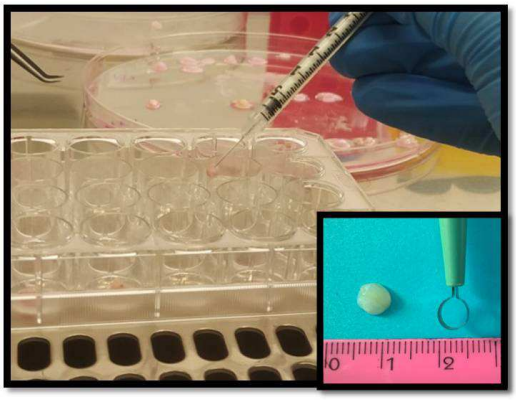

Figure 5: Representation of dimension of the decellularized sample and recellularization setting.

3.6 Drug treatment and cytotoxicity assay

For the 5-FU treatment in the 3D setting, N and T scaffolds were seeded with $2.5x10^5$ CRC cells in 24-well plates. Five days post seeding, the cells were treated with 1 µM, 10 µM and 100 µM 5-FU for 72 h. For the 5-FU treatment of the 2D cultures, HT29 were seeded at $5x10^3$ cells per well in 96-well plates and treated with different concentrations of 5-FU from 0.1 µM to 1000 µM for 72 hours. Cell viability was determined 24 h, 48 h and 72 h post-treatment by reading the absorbance using the Multilabel Plate Reader VICTOR (PerkinElmer, Waltham, MA). The treatment response for each culture setting was standardized to the corresponding untreated cultures. Similarly, the PrestoBlue Cell Viability Reagent was used for the Inhibitory Concentration 50% (IC50) determination using GraphPad Prism software 6.

3.7 Determination of cells' proliferation rate

The 5-ethynyl-2'-deoxyuridine (EDU)–Click kit was used for the evaluation of DNA synthesis following the manufacturer's instructions. The cells were pulsed with EdU for four hours before fixation in 4 % PFA and subsequent EdU detection. Nuclei were counterstained with DAPI (Sigma-Aldrich). EdU-positive cells were counted under an inverted fluorescence microscope (BMI6000B, Leica) and normalized to the total number of nuclei.

3.8 Fluorescent cell labeling, zebrafish embryos preparation and tumor cell implantation

The Tg(fli1: EGFP) zebrafish embryos [86] were raised, staged and maintained as already described [87]. Dechorionized, two days post fertilization (dpf) zebrafish embryos were anaesthetized with 0.003% tricaine (Sigma-Aldrich) and positioned on a 10 cm Petridish coated with 3% agarose. Non-fluorescent HT29 cells were labeled with the Vybrant® DiI Cell-Labeling Solution (Invitrogen) according to the manufacturer’s instructions. The fluorescent HT29 cells were then resuspended in PBS and implanted using borosilicate glass capillary needles (OD/ID: 1.0/0.75 mm, WPI), a Pneumatic Picopump and a micro-manipulator (WPI). Approximately 200 cells were injected within the duct of Cuvier of each anesthetized embryo. After the implantation, zebrafish embryos were maintained at 33°C. The animals showing less than 100 cells after 2h post-injection were discarded from the analysis. At least 50 embryos per group were analyzed from three independent experiments. Embryos were live photographed using a BM6000 (Leica) microscope equipped with a PerkinElmer UltraVIEW VoX Confocal System.

3.9 Scanning electron microscopy (SEM)

Samples were fixed with 2 % glutaraldehyde in 0.1 M phosphate; following washing they were cut into segments of approximately 1 cm length and cryoprotected in 25 % sucrose, 10 % glycerol in 0.05 MPBS (pH 7.4) for 2 h, then fast frozen. At the time of analysis, samples were placed back into the cryoprotectant at RT and allowed to thaw. After washing, the material was fixed in 1 % OsO4/0.1 M phosphate buffer (pH 7.3) and washed again. After rinsing with deionized water, specimens were dehydrated in a graded ethanol-water series to 100 % ethanol, critical point dried using CO2 and finally mounted on aluminum stubs using sticky carbon taps. Samples were mounted and coated with a thin layer of Au/Pd (approximately 2 nm thick) using a Gatan ion beam coater. Images were recorded with a Jeol 7401 FEG scanning electron microscope.

3.10 Permeability tissues evaluation

In the permeability measure method, both biological and synthetic specimens were evaluated. A device was adopted for the tissue permeability measurement (Figure 6A-B). Tissue samples were confined in cylindrical space with diameter of 3 mm and thickness of 2 mm. Two porous metal plates were placed in the upper and lower surface to fix the samples and allow the fluid filtration. The upper metal plate was connected to a pipette with internal diameter of 6 mm and total height of 250 mm. The permeability of a sample was estimated filling the pipette with fluid at an initial height of 210 mm, with respect to the inferior surface of the specimen. The lower surface of the sample was subjected to atmospheric pressure, while the upper surface to variable relative pressure depending on

the height of the fluid column. In this condition, it can be assumed that the filtration in the specimen is governed by Darcy's Law:

$$Q = KA_s \frac{\gamma H(t)}{\Delta x} \tag{1}$$

where Q is the flux of the fluid, K the coefficient of permeability of the tissue to the permeating fluid, A_s the transversal section of the specimen, γ the specific weight of the fluid, $H(t)$ the height of fluid column over time t and Δx the thickness of the specimen. Defined with A_p the transversal section of the pipette and considering the continuity equation between pipette and sample, the Darcy's Law can be integrated over time and rewritten as follow:

$$H(t) = H(t_0)\exp\left[-K\frac{A_s}{A_p}\frac{\gamma}{\Delta x}(t-t_0)\right] \tag{2}$$

where t is the current time and t_0 the initial time of the filtration process.

In the experiments, the fluid column height was acquired over time. In all the experiments this height was included in the range of 210-100 mm, corresponding to a pressure gradient in the specimen of 1.03-0.49 kPa/mm. Fluid column height vs. time experimental data of each specimen were then fitted by equation (2), where the only unknown parameter is the permeability of the tissue K. The fitting procedure was implemented by means of a user-defined procedure in (Scilab 5.5.2, ESI Group, France), minimizing the mean square error between numerical results and experimental data.

$$\Xi = \frac{1}{N}\sum_{i=1}^{N}\left[1-\frac{H(t_i)}{H_{i,exp}}\right]^2 \tag{3}$$

where N is the number of experimental data acquired, $H_{i,exp}$ the experimental value obtained at time t_i and $H(t_i)$ its estimation through equation (2). Each sample was then characterized by the specific value of permeability found from the fitting.

Before to proceed with the measurement of the permeability of native and decellularized tissues, experimental device and fitting method were tested on samples of a rough porous polymeric material, in order to estimate the reliability of the proposed approach. In detail, we repeated the permeability measurement on the same sample 5 times. The permeability measurement was then taken on 8 different samples of the same material (Figure 6C).

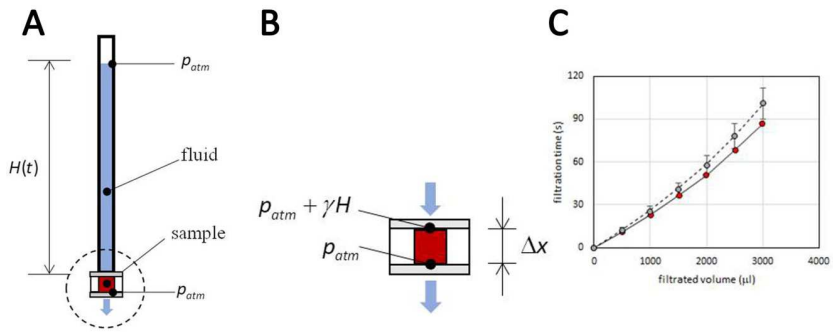

Figure 6: Device adopted for the tissue permeability measurement.
-Fig 6A drawing of permeability device
-Fig 6B enlargement of the section where the sample is deposited to measure permeability
-Fig 6C rough porous polymeric material permeability measurement

3.11 Flow cytometry analyses

Cell surface antigen expression was analysed by flow cytometry using cultivated cells after detachment by trypsin5 mM Na-EDTA in PBS ph7.5. Briefly, cell suspensions were incubated with 5 mL of antibody for 20 minutes at 4 °C in the dark. After a washing step, cells were resuspended in 1X PBS; acquisition and analyses were performed using FACS CantoII (Becton Dickinson). The antibodies used were: anti-MHCII:APC, anti-CD86:PE, anti-CD206:BB515, CD14:PerCP/Cyanina5.5, anti-CD68:PE (all from BD Bioscience). eFluor 780 (eBiosciences) was used as viability assay.

3.12 Statistical analysis

All graphs and statistical analyses were performed using the GraphPad Prism Software 6. Data were expressed as means ± SEM. For the comparison of coupled experimental groups, the two-sided Student's t-tests (for parametric dataset) and Mann-Whitney test (for non-parametric dataset) were used. One-way ANOVA with Bonferroni's post-test (for parametric dataset) and Kruskal-Wallis test with Dunns post-test (for non-parametric dataset), were performed for multiple comparisons. A p-value < .05 was considered statistically significant (*: p-value < .05; **: p-value < .01; ***: p-value < .001).

4.RESULTS

4.1 Characterization of repopulated 3DN and 3DT models

Biopsies of resected primary CRC and matched healthy counterpart were obtained and decellularized as previously demonstrated by our research group [88] to generate normal (3DN) and tumor (3DT) scaffolds. The qualitative and quantitative characterization of matched HT29 recellularized samples from 3DN and 3DT specimens were performed through histological, immunofluorescences and DNA amount quantification.

HT29 adenocarcinoma-derived cells cultured in 3DN and 3DT scaffolds were uniformly distributed, initially occupying the outermost part, and then penetrating inside the scaffolds. Nuclei were clearly visualized with reasonable size and no signs of cellular suffering. The cells populating the tumor scaffolds were organized in a rounded configuration that, according to their origin and microenvironment structure, is characteristic of colic crypts (Figure 7A). The H&E staining revealed a large number of spherical cell aggregates that repopulated the porous spaces within the scaffolds (Figure 7A). These round gland-like aggregates strongly adhered to the ECM composing the scaffolds. Both Masson Trichrome and Collagen IV stains underlined a uniform presence of collagen fibers that were equally distributed in 3DN and in 3DT tissues (Figure 7A). The periodic acid–Schiff (PAS) staining evidenced the presence of secreted and organized glycosaminoglycans and glycoproteins (Figure 7A). In addition, PAS staining showed that HT29 cells injected in both recellularized healthy and tumor tissues, actively produced and secreted mucus. Quantification of DNA of the fresh tissues and repopulated 3D constructs, both from healthy and tumor specimens after 5 days of culture, showed a complete different cellular content in respect to decellularized specimens (p-value =

0.0073 and p-value = 0.0073, respectively). In fact, the repopulated scaffolds showed a partial restoration of the amount of DNA, accounting for respectively 1/5 in 3DN compared with the healthy fresh samples and 1/4 in 3DT compared with tumor fresh tissues (Figure 7B).

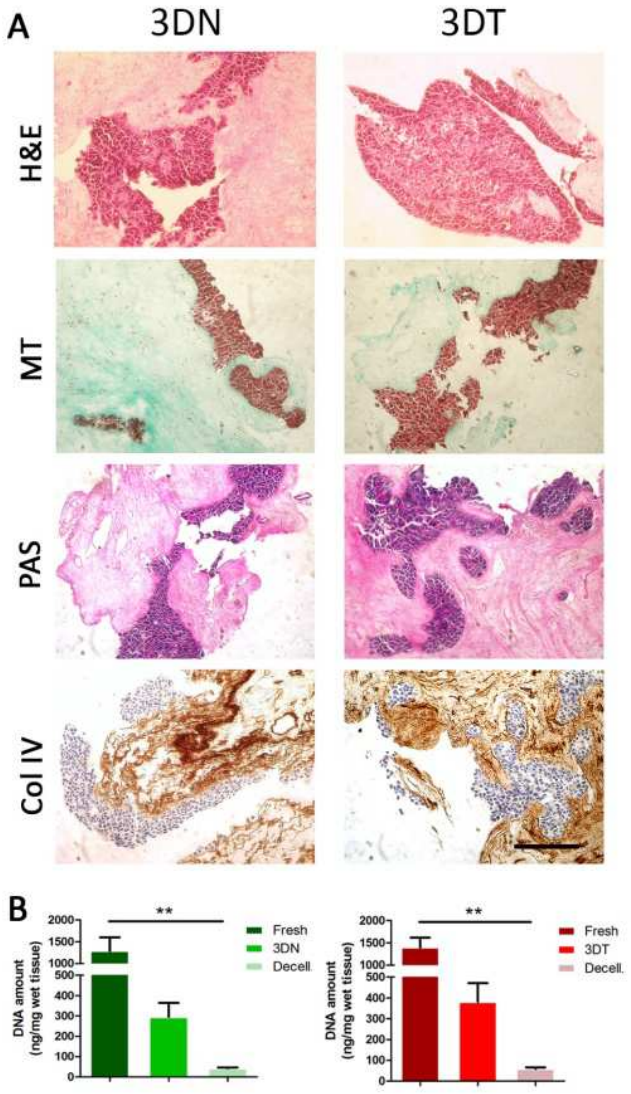

Figure 7: Characterization of matched HT29 recellularized samples from 3DN and 3DT specimens:
-Fig 7A histological characterization of sections stained with Haematoxiline and Eosine (H&E), showing glandular-like cells organization within the scaffold; Masson's trichrome (MT) and collagen IV staining (Col IV), enabling the detection of collagens; Periodic Acid-Shiff (PAS), evidencing glycosaminoglycan and glycoprotein (scale bar = 200µm).
-Fig 7B DNA amount quantification (by spectrophotometer) in fresh samples, after decellularization process and after 5 days of repopulation with HT29, in both 3DN and 3DT. (**: p-value < .01)

4.2 Evaluation of proliferation and polarization of HT29 cultured cells into 3DN and 3DT

To test the ability of decellularized scaffolds to support cell viability, we evaluated the proliferation index of the injected HT29 cells through the Ki67 proliferation marker (Figure 8A). As showed in the figure, the number of Ki67-positive cells in 3DT specimens (80%) was significantly higher (p-value =0.0180) compared with 3DN (55%) at day five of culture. Furthermore, as previously highlighted by the literature [89-91], immunofluorescence analysis evidenced fewer proliferating cell in the 3D model compared with cells grown in conventional 2D conditions. Since the adhesion and cytoskeletal molecules play a vital role in cell morphology and function, we investigated whether the expression and localization of E-Cadherin and Vimentin molecules differed among cells cultured in 3DN, 3DT and 2D conventional culture setting. The typical epithelial-like tumor phenotype of HT29 cells observed within the 2D standard cultures condition was fully preserved in both the repopulated 3DN and 3DT, as evidenced by the high expression of the epithelial cell adhesion marker E-Cadherin (93.5 % in 3DN and 91.8 % in 3DT) and the very low expression of the mesenchymal adhesion molecule Vimentin (3.6 % in 3DN and 4 % in 3DT) (Figure 8A-B) [92-93].

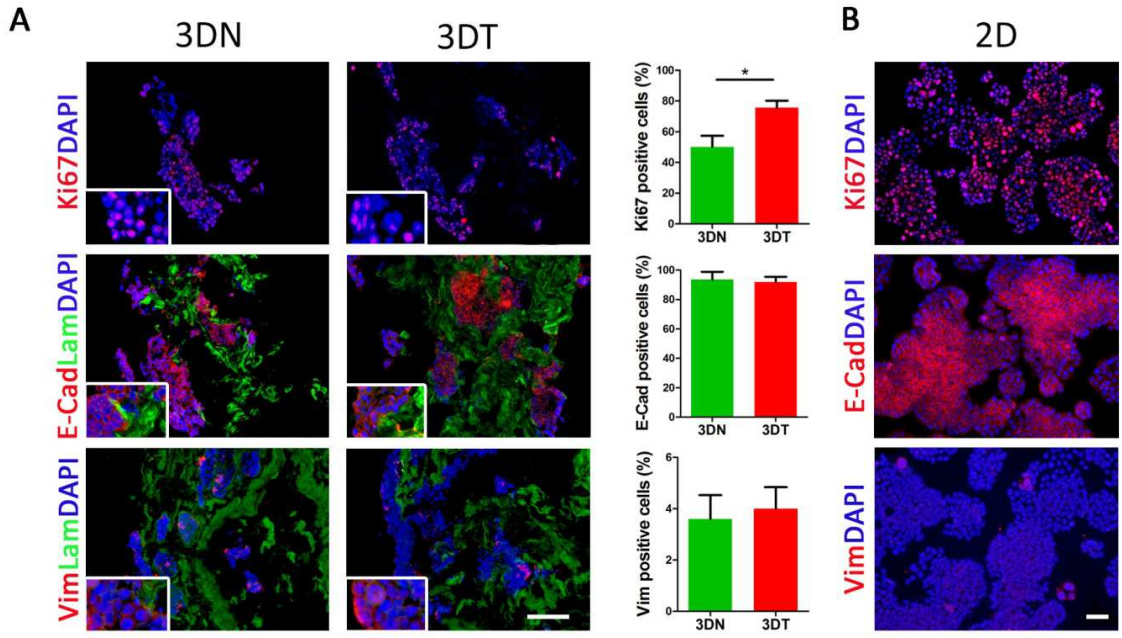

Figure 8: Evaluation of proliferation and polarization of HT29 in 3D-N and 3D-T
-Fig 8A immunofluorescence stainings in 3DT and 3DN: Ki67, as proliferation marker; E-cadherin as epithelial marker; Vimentin, as mesenchymal marker; Laminin to highlight basement membrane structure; DAPI to counterstain nuclei (scale bar= 100µm)(*: p-value < .05)
-Fig 8B immunofluorescence stainings in 2D (scale bar= 50 µm).

4.3 Effect of 5-FU treatment on cells cultured in 2D and 3D model

5-FU is a widely used drug in CRC adjuvant chemotherapy and still represents the backbone of different multimodal treatment [94]. Firstly, we tested whether the IC50 for 5-FU determined *in vitro* in cells cultured for 72h of treatment was similar to what previously determined by Choi and colleagues (1µM). (Figue 9A-B) [95].

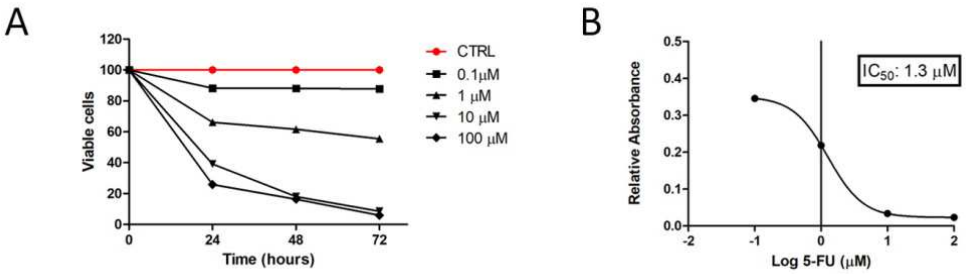

Figure 9: Effect of 5-FU treatment on cells cultured in a conventional 2D model:
-Fig 9A evaluation of drug sensitivity to 5-FU in HT29 2D culture using absorbance fold change detection (indicating cell viability).
-Fig 9B 5-FU 2D IC50 calculation by nonlinear regression.

Secondly, we compared the efficacy of 5-FU treatment in 2D conventional HT29 cell culture, 3DN and 3DT culture models. In accordance with the 2D model, response to 5-FU in 3DN and 3DT models maintained a dose-related trend (Figure 10A). When compared to the 2D conventional culture, HT29 cells grown in both 3DN and 3DT models displayed a reduced sensitivity to 5-FU (3DN vs 2D: p-value < 0.0001 at 1-10-100 µM; 3DT vs 2D: p-value < 0.0001 at 1 and 10 µM; p-value < 0.01 at 100 µM), with an increased IC50 of about 10-fold (IC50 = 11.58 µM) (Figures 10A-B). The IC50 value in 3DN and 3DT models was further confirmed by additional immunohistochemistry analyses. Indeed, MIB1-positive cells, proliferation marker, showed a significant decrease of about 50% in both the 3DN and 3DT when treated with 5-FU 3D IC50 (3DN p-value = 0.0089; 3D-T p-value < 0.0001) (Figure 10C).

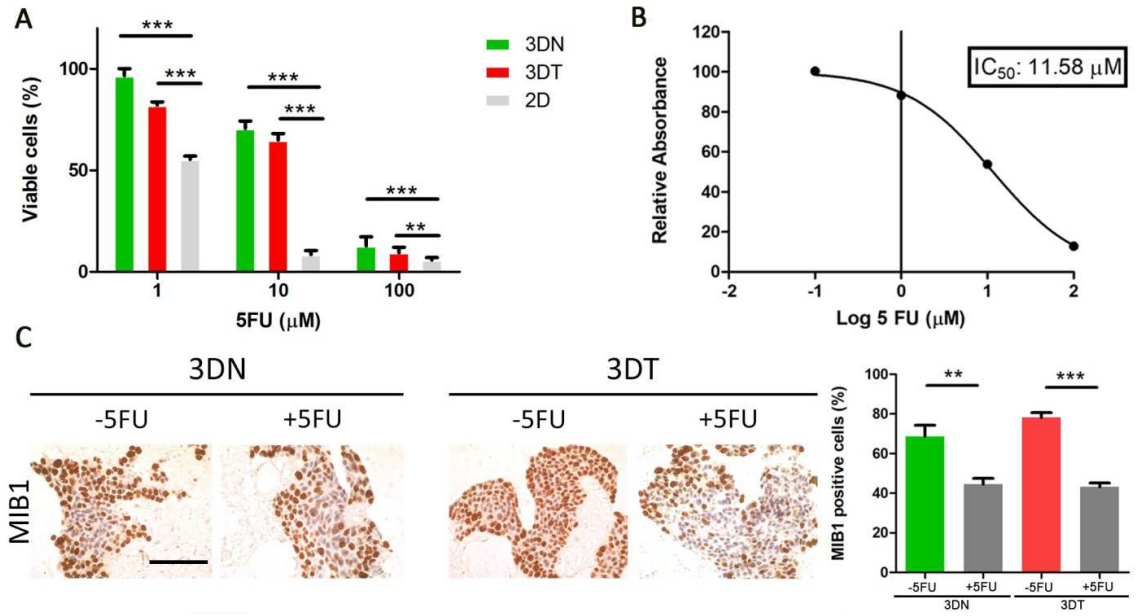

Figure 10: Effect of 5-FU treatment on cells cultured in a 3D model
-Fig 10A comparison between percentages of viable cells (by absorbance fold change detection) after administration of 5-FU at 1-10-100 µM in a 2D culture and in both 3DN and 3DT models (**: p-value < .01; ***: p-value < .001).
-Fig 10B calculation of 5-FU 3D IC50 by nonlinear regression.
-Fig 10C MIB1 immunohistochemistry before and after administration of 3D-calculated IC50 in both 3DN and 3DT; comparison of percentages of $MIB1^+$ cells before and after treatment (scale bar= 100 µm) (**: p-value < .01; ***: p-value < .001).

To evaluate the cell response after colonization of a complex biologic environment, as represented by our 3D culture model, we investigated HT29 cell death after specific (5-FU) or non-specific induced stress (biologic environment). The EdU and Tunel assays were used for the detection of cell proliferation and apoptosis, respectively. We identified a significant proliferative phenotype in non-treated 3DN and 3DT models (56.6 % and 61.5 % of EdU-positive cells; 2.1 % and 1.9 % of Tunel-positive cells), a situation that was completely reversed after 5-FU treatment with the calculated 3D IC50 (15.5 % and 12.7 % of EdU positive cells; 45.5 % and 29.6 % of Tunel positive cells) (Figures 11A-B). These findings underlined the healthy behavior of HT29 cells cultured in 3D models and their sensitivity to standard chemotherapy treatment.

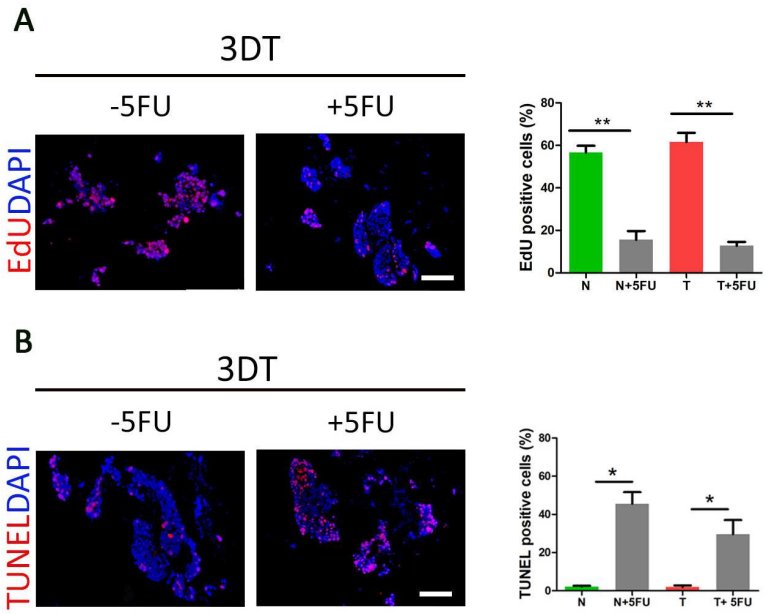

Figure 11:Evaluation of cell proliferation and apoptosis in 3DT
-Fig 11A EdU fluorescent staining as markers of proliferation, before and after 5-FU treatment in 3DT; comparison between percentages of EdU^+ cells on the total, before and after treatment in 3DN and 3DT. (**: p-value < .01).
-Fig 11B TUNEL assay, as markers of apoptosis, before and after 5-FU treatment in 3DT; comparison between percentages of $TUNEL^+$ cells, before and after treatment in 3DN and 3DT (scale bar=100 µm) (*:p-value < .05).

4.4 Generation of a zebrafish (*Danio rerio*) xenotransplantation model

To compare the *in vitro* results with an *in vivo* model, we generated a zebrafish (*Danio rerio*) xenotransplantation model (Figure 12A). We monitored the cells for 72 consecutive hours after injection to evaluate the cell viability and we decided to exclude from the following experiments the 72 h timepoint sincewe found a cell survival rate inferior to 50% (Figure 12B). For this assay, the HT29 cells were injected into the duct of Cuvier (white asterisk in Figure 12A) of Tg(fli1:EGFP) embryos with vessels marked in green, as previously described by Aveic et al. [96]. Cells labeled with Dil live cell tracer rapidly distributed throughout the vasculature of the injected embryos. Cells were able to

invade different anatomical districts such as gut, pericardical cavity, tail and caudal region (Figure 12C). Morover, we observed phenomena of extravasation and metastasis formation (Figure 12D).

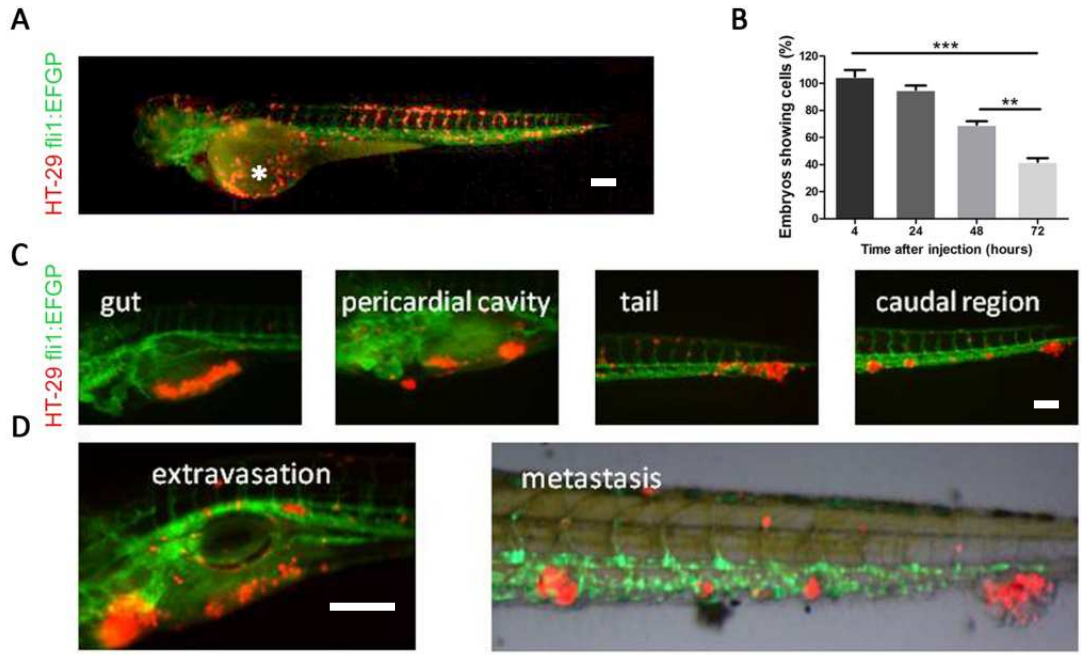

Figure 12:Generation of a zebrafish (*Danio rerio*) xenotransplantation model
-Fig 12A Tg(fli1:EGFP) zebrafish embryo (with green fluorescent vessels) xenotransplantated with Dil marked HT29 cells (red), injected into the duct of Couvier (white asterisk). Visualization under confocal microscopy (scale bar= 100 µm).
-Fig 12B monitoring of zebrafish embryos showing viable cells after 24-48-72 h post injection. (**: p-value < .01; ***: p-value < .001).
-Fig 12C-D different anatomical districts invaded by Dil^{+} cells (scale bar=200 µm). Phenomena of extravasation and metastasis formation in xenotransplantation model (scale bar=250 µm).

4.5 Effect of 5-FU treatment on *in vivo* zebrafish model

To investigate the concentration sufficient to remove at least half of the injected cells and compare it with that obtained in 2D and 3D setting, we incubated the xenotransplanted zebrafish with 5-FU directly administered into the embryo medium. In order to compare the effects previously observed in the 2D and 3D models, we used the IC50 calculated in

2D and 3D cultures, respectively. We evaluated the fluorescence fold change in the caudal region of each injected embryo after 24 and 48 hours of treatment (Figure 13A-B). Interestingly, we observed a significant reduction of Dil-tumor cells only in embryos treated with 3D IC50 concentration if compared with control (DMSO-treated embryos) in particular after 48 hours of treatments (p-value = .0027) (Figure 13B). These data suggest that the effects observed with our *in vitro* 3D model recapitulate the *in vivo* zebrafish chemoresponse.

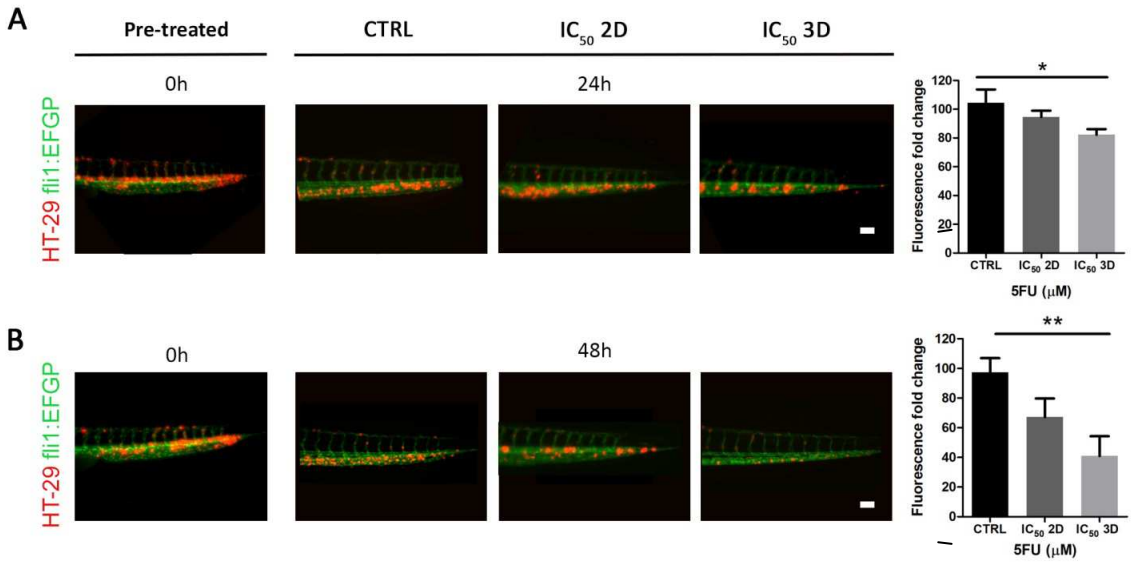

Figure 13: Effect of 5-FU treatment on *in vivo* zebrafish model
-Fig 13A analysis of Dil HT29 injected cells in zebrafish embryos, pre-treatment (time 0), and after 24 h of treatment with DMSO (control group); IC50 2D and 3D 5FU concentrations and quantifications. (scale bar= 100µm) (*: p-value < .05).
-Fig 13B analysis of Dil HT29 injected cells in zebrafish embryos, pre-treatment (time 0), and after 48 h of treatment with DMSO (control group); IC50 2D and 3D 5FU concentrations and quantifications.(scale bar= 100 µm) (**: p-value < .01).

4.6 Patient derived scaffold permeability evaluation

To confirm that the pharmacological effect observed in our 3D model was not linked to an intrinsic cellular suffering, but to a real drug absorption by the injected cells, we analyzed patient derived scaffold permeability, drug diffusion and localization when

administered to a 3D construct. To verify the drug absorption, we recellularized tumor scaffolds with HT29 GFP-positive cells for 5 days and then we added the Doxorubucin (doxo). The decision to use Doxorubicin arises from the possibility to exploit and measure its autofluorescence (emission wavelength: 594 nm) through confocal microscopy analysis [97]. After 3 days of treatment, we observed a high percentage (76%) of GFP^+ cells and doxo co-localized events (Figure 14A-B-C). Importantly, these co-localizations were not only present on the top of the scaffolds but also in its inner core (Figure 14A). In addition, we noticed that the drug specifically penetrated cell nuclei and did not bind the ECM (Figure 14D).

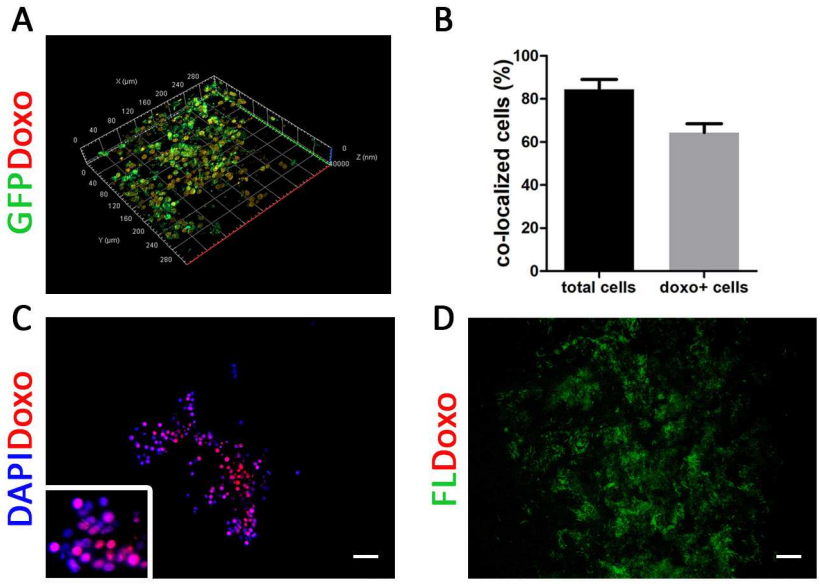

Figure 14: Drug diffusion evaluation
-Fig 14A Doxorubicin (red) diffusion assay in 3DT, repopulated with HT29. GFP^+ cells (green).
-Fig 14B quantification of co-localize cells
-Fig 14C confirm in Immunofluorescence of co-localization (scale bar= 100µm)
-Fig 14D immunofluorescence of FL/Doxo (scale bar= 100µm)

As previously reported in literature [98] the decellularization process leave biological tissues rich in pores and spaces left empty by the nuclei, as clearly visible also from our SEM analyses (Figure 15A). We observed a significant increasing permeability in tumor

decellularized tissue compared to tumor fresh (p-value=0.036) (Figure 15D). In figure 15 are reported the experimental results of the filtration process carried out on the two types of tumor colon tissues (fresh and decellularized) (Figure 15C). The data, obtained through a simple device described in Figure 15B with Computer-Aided Design (CAD), are reported in terms of volume filtrated through the specimen (µl) versus filtration time (s). Open circles refer to the experimental values and solid black lines to the equation (2) fitted to experimental data and the charts report the estimated values of permeability K (mm^4/Ns) (Figure 15C). The estimation of the filtration process was generally acceptable for all the samples, but with large variability of the estimated permeability within each group, as shown by Table 5, where are all the permeability values are reported with average permeability and standard deviation (SD).

	Tissue permeability K (mm^4/Ns)			
Sample #	**HF**	**TF**	**HD**	**TD**
1	1.6	96.5	43.3	1189.4
2	10.5	148.0	16.1	3102.4
3	17.3	36.1	281.3	6323.6
4	-	-	2582.1	3887.2
5	-	-	1666.6	-
Average	9.8	93.5	917.9	3625.7
SD	4.1	55.9	1048.3	1430.3

Table 5: Estimated values of permeability on the different types of tissue
HF: Healty colon Fresh, TF: Tumor colon Fresh, HD: Healty colon Decellularized, TD: Tumor colon Decellularized. (SD:standard deviation).

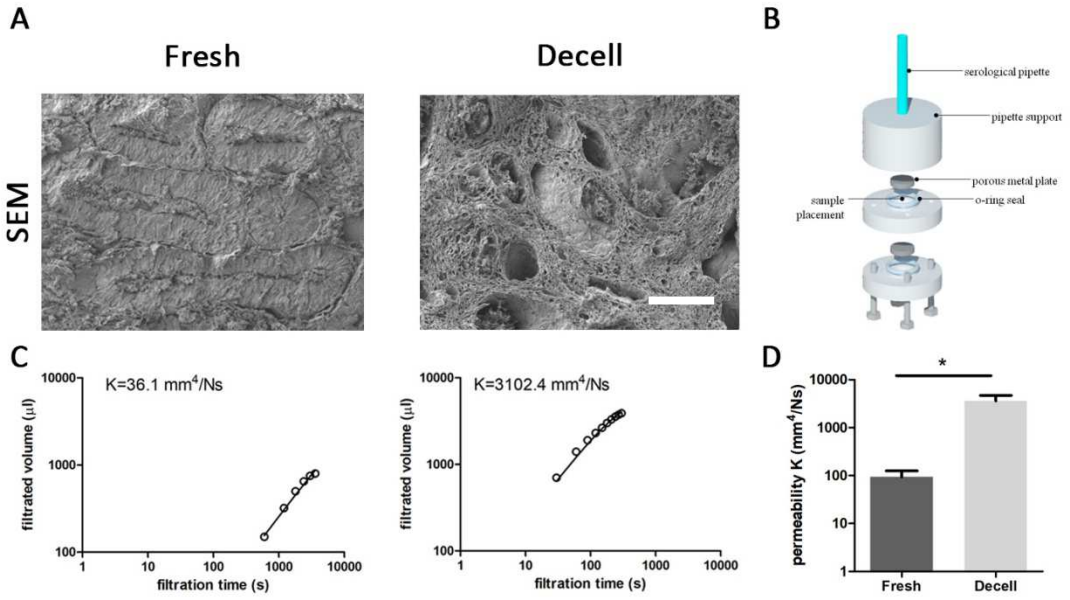

Figure 15: Tumor tissue permeability evaluation:
-Fig 15A scanning electron microscopy (SEM) analysis performed for tumor colon fresh and decellularized (decell) (Scale bar= 100 µm)
-Fig 15B drawing in Computer-Aided Design (CAD) of permeability device
-Fig 15C experimental results of the filtration process carried out on the tumor colon fresh (mean square error between numerical results and experimental data resulted 0.027). and decellularized (decell) (mean square error between numerical results and experimental data resulted 0.020).
-Fig 15D quantification of permeability measurement obtained from Tumor colon fresh and decellularized (decell) (*: p-value < .05).

4.6 Tumor extracellular matrix educating newly recruited monocytes

One of the most abundant tumor-infiltrating cell population is represented by tumor-associated macrophages (TAMs) [99]. Considering that tumor-infiltrating macrophages, at least in part, derive from newly recruited monocytes [100], we evaluated the contribution of tumor ECM in driving macrophages differentiation and polarization and its impact on their antigen presentation ability. We exposed monocytes derived from buffy coat obtain from donor patients to healthy and tumor decellularized matrix for 5 days. Interestingly, after 5 days monocytes lost the expression of CD14 lineage marker in favor of the expression of CD68 macrophages' marker (Figure 16A). Cells exposed to

tumor decellularized matrix acquired a pro-tumoral anti-inflammatory profile characterized by the increased expression of CD206 (a marker expressed by M2 and pro-tumoral macrophages) (Figure 16B) and decrease expression of both histocompatibility complex type II (MHC-II) and CD86 (two markers expressed by M1 macrophages) compared to cells exposed to normal matrix (Figure 16C-D). These data suggest that the tumor ECM exerts a crucial role in educating newly recruited monocytes towards a pro-tumoral macrophage-like profile.

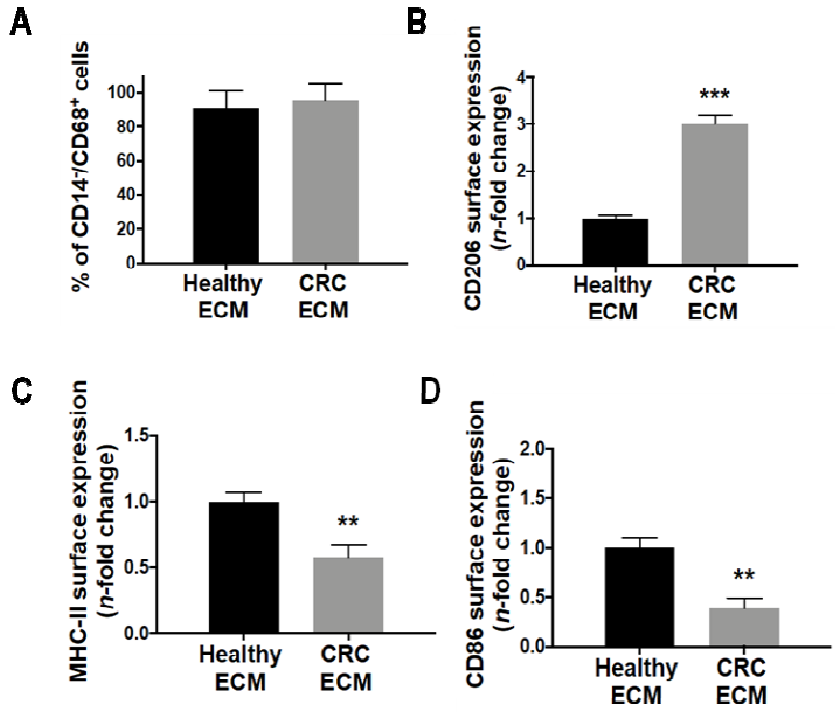

Figure 16: Analysis of macrophages lineage marker

-Fig 16A ratio between CD14 (monocytes lineage marker) in favor of the expression of CD68 (macrophages lineage marker)

-Fig 16B-C-D flow cytometry fold chanche evaluation in Healthy and Tumor ECM for CD206 (a marker expressed by M2 macrophages), MHC-II and CD86 (markers expressed by M1 macrophages) (**: p-value < .01; ***: p-value < .001).

5.DISCUSSION

The majority of high risk stage II and III CRC patients, both young and adults, do not completely benefit from receiving standard chemotherapy during adjuvant treatments because they have either already been cured by surgery or because their tumor cells are resistant to the chemotherapy. For these patients, the benefit of adjuvant chemotherapy remains under debate [101-102]. Moreover, the success rate for many drugs evaluated in different conventional cellular models and animal models tested in clinical trials is very low [103]. The development of new *in vitro* models that could be useful for drug screenings and capable of faithfully mimic the clinical response and predicting the future success of specific drugs, is one of the most important unmet needs in the field of cancer therapy. This argument becomes even more important in the pediatric context where there are still no guidelines for colon cancer treatments and where experimental approaches or studies of personalized medicine are conditioned by the unavailability of biological material. There is a robust body of evidence in adults, but studies of pediatric CRC have been limited by small numbers of patients, with no large institutional experience or prospective studies to guide treatment [104-106]. Despite the small numbers, studies demonstrated differences between pediatric and adults CRC patients, showing a significantly higher proportion of aggressive histology, particularly signet ring and mucinous and a higher proportion presenting with metastatic disease [107-108]. In 2016 in Journal of Pediatric Surgery Gabriela C. Poles claimed that "*Currently there are no specifically pediatric CRC treatment algorithms, so adult protocols are utilized, but in the absence of prospective trials it is unclear if this is the best option or how age affects individual treatment decisions"*. In this context, an urgent need not yet addressed is the

random assignment to adjuvant chemotherapy without any predictive factor of efficacy. In the field of drug discovery, the critical step is the preclinical evaluation. To identify new drugs, thus trying to shorten the *in vitro* pre-clinical testing phases, the scientific community is evaluating the three-dimensional culturing approach as a way to bridge the gap between the *in vitro* and *in vivo* experimental phases. A limit to the definition of a 3D model is certainly the fact that many ideas are associated with this acronym. 3D, for examples, is associated with multicellular spheroids, organoids, synthetic scaffolds, hydrogels, organs-on-chips, and 3D bioprinting each of them with their own advantages and disadvantages [73]. In a very recent work Vlachogiannis et al., for example, presented a deeper characterization of a living biobank of gastrointestinal carcinomas patient derived organoids (PDOs) and they demonstrated histological and molecular-mutational overlapping between the *in vivo* cancer and *ex vivo* model [109]. In addition they were able to capture spatio-temporal intratumor heterogeneity, when established from multiple biopsies at the time of disease progression and when compared with those established at the beginning of treatment. This concordance has been extensively confirmed by genomic and transcriptomic profiling [109]. Nevertheless, we believe that the use of organoids is still too tied to a vision that associates the cancer disease with a cellular-only disease.

Microenvironment co-evolves into an activated state through continuous paracrine communication, thus creating a dynamic signaling circuitry that promotes cancer initiation and growth, and ultimately leads to a fatal disease. Indeed, many of the hallmarks of cancer delineated by Hanahan and Weinberg are provided by various stromal components, including ECM, endothelial cells, fibroblasts, leukocytes [110]. Growing evidence indicates that ECM is not only a physical support for the cells but also as an active component of tumors, implicated in response to therapy [111].

In our opinion, the best way to recreate a concrete *in vitro* 3D preclinical model useful for drug evaluation consist in the creation of a complete biological model without the introduction of any synthetic component. Using regenerative medicine principles, our goal was to re-create *in vitr*o a prototype of pathological tissue genetically compatible with the patients of origin.

In this thesis, a patient-derived ECM contributed to reproduce the specific patient microenvironment and we used it for evaluating (1) use of ECM scaffolds as a support for tumor cell growth and proliferation, and (2) the chemo-sensitivity in three different settings with increasing biological complexity: the 2D conventional culture plate, the 3D CRC model, and the *in vivo* zebrafish model.

We developed a decellularized protocol, recently reported by our team [88] that combines the use of a sodium deoxycholate and DNase in order to obtain an acellular ECM to be used as a scaffold to analyze cell behavior. The methodology we reported was applied to healthy human colon mucosa and match CRC biopsies from the same patient. Thanks to the immunofluorescence and immunohistochemistry analysis, we observed that the collagens and glycosaminoglycans were properly maintained and distributed within the scaffold also after the DET process [88]. The importance of the ECM in maintaining the tissue homeostasis is exemplified by the study of Weaver et al. [112] in which they reverted the malignant phenotypes of breast cancer cells to the wild-type phenotype. They achieved this by culturing breast cancer cells onto basement membrane-based 3D substrates coated in integrin β1-blocking antibodies. This study confirmed that the crosstalk between the ECM and the populating cells is able to reverse the cancer phenotypes, emphasizing the ECM's role in maintaining the correct cell phenotype. To evaluate the ability of the ECM to sustain cancer cell maintenance, we used adenocarcinoma grade II stabilized cells, the HT29 cell line. According to Genovese and

colleagues, in the 3DT we observed that tumor cells were located inside the crypts and on the top of the luminal area. Moreover, immunohistochemistry analyses revealed that tumor cells acquired different phenotypes based on their location into the ECM. The cells inside the crypts are more rounded and organized to create a lumen in the center, the cells that are placed on the top of the luminal area are thinner in order to create a multi-layer structure following the anatomical morfology of colon cells. In accordance with Friedrich et al ,we observed that cells in the outer layer were in active proliferation due to adequate access to nutrients and oxygen, simulating the *in vivo* vascularized region of the tumor close to the capillaries [113].

In our 3D system, in particular in the tumor setting, the matrices sustained cell differentiation of HT29, such as the formation of glandular-like structures and expression of mucus underline by the intense purple staining in close proximity to the tumor cells inside the ECM. The expression of mucus is a marker of functional differentiation of epithelial cells injected into the ECM, since the only cells grown in the standard 2D petri dish are known to have no mucus-secreting properties [114]. These findings emphasized the capability of ECM components to sustain the differentiation phenotype of HT29 cells.

In this study, we demonstrated that the 3D CRC model exhibited reduced sensitivity to 5-FU treatments compared with conventional 2D cultures.

The fact that numerous anticancer drugs were subsequently discarded during the clinical evaluations indicated that the anticancer activity tends to be overestimated on a 2D-culture-based screening platform [115]. We decided to use the biopsy-derived ECM not only as a physical scaffold for maintaining the structural integrity of the tissue but also as a reservoir of biochemical and biophysical signals to support cell growth during the recellularization process. The differential drug sensitivity observed between 2D and 3D cultures could be attributed to the decreased compound access or reduced drug sensitivity

in response to hypoxic and more slowly cycling cells under 3D culture conditions [30] [116] [117]. However, the exact signaling mechanism implicated in drug resistance in 3D platforms is still unclear. Saraswathy and Gong worked on the study of the interplay among various factors (e.g. intracellular changes, paracrine signaling, modifications in the supporting matrix) that may contribute to the reduced drug sensitivity in 3D cultures. In particular, the hypoxia in cancer is known to lead resistance via different pathways such as the lost of p53-mediated apoptosis and the enhanced P-glycoprotein expression [118].We performed a diffusion assay in confocal microscopy with Doxorubicin, cytostatic chemotherapeutic drug used in treatment of a wide variety of cancers. Exploiting its natural autofluorescence the assay demonstrated the co-localization of Doxorubicin with cells, even in the deep parts of the scaffold. Same diffusion pattern is presumed also for 5-FU, since it presents a molecular mass even much lower than Doxorubicin (Doxorubicin molecular mass: 543.52 g/mol and 5-FU molecular mass: 130.077 g/mol.) suggesting the effective drug penetration in the scaffold. For this reason we hypothesize that the apoptosis observed was linked to 5-FU pharmaceutical effect, and not to a casual stress. Taking advantage of the fluorescence of Doxorubicin, we ascertained that drug also penetrated the innermost space of the 3D model, staining the cellular nuclei. In the therapeutic regime to date, a mono-therapy with 5-FU leads to a limited treatment response and to unsatisfactory results in most of the cases. Therefore, 5-FU is mostly applied in combination with other molecules. We have recently begun to exploit new combinations drug among the most used in clinical practice such as 5-fluorouracil (FU) + oxaliplatin + folinic acid (FOLFOX) and 5-fluorouracil (FU) + irinotecan+ folinic acid (FOLFIRI) [119].

In order to compare our results obtained with the 3D model with an *in vivo* model, we successfully generated a xenotransplanted zebrafish model. We considered several

advantages using the zebrafish embryos: the short generation time, the fast and external embryonic development, the large number of offspring, and most importantly the transparency of the embryos which enables live and noninvasive fluorescent imaging [120]. Many researchers are translating drug screening platforms from the mouse model to the zebrafish, as in the work of Fior et al. in which they performed proof-of-concept experiments in which assessed the main therapeutic options of the CRC guidelines. The zebrafish xenotransplantation model was generated through injecting the patient-derived human colorectal cancer cell lines. In this experimental set, we could see that the model proposed by our group provides IC50 completely comparable with the previous published *in vivo* model, providing greater robustness and accuracy to our patient-derived *in vitro* 3D model.

The mechanics of permeability (K) were first described by groundwater hydrologists, starting in the 1850s with Henry Darcy in Dijon, France, where his work as a engineer

The formula that he derived and that we applied is commonly referred to as Darcy's law.

As it is reported in literature we showed that the permeability increases in the tumoral tissues compared to the healthy, and it is interesting to note how this trend is maintained not only in the fresh tissues but also in decellularized tissues [121]. Permeability depends on many factors, such as pore size, matrix composition, and matrix geometry. We estimated the increased permeability of decellularized tumor samples in respect to the original fresh tissue in order to understand how easily these scaffolds could allow the uptake of both key factors for cell survival (nutrients, oxygen etc ...) and exogenous or harmful factors such as drugs. We believe that, although repopulated by the cells, our 3D model can be effectively perfused by drugs and can therefore be a useful preclinical model for the study of drug delivery. In efforts to recreate a physiological model we evaluated the relationship between ECM and immune cells, in particular, in the

microenvironment of solid tumors, macrophages are the most abundant immune component. Their presence correlates with worse prognosis in several cancers included colon cancer [122]. In 2017 Pinto and coworkers investigated CRC's ECM, macrophage polarization and how this impacts on cancer cell invasion [81]. In our 3D model, similarly to what described by Pinto et al., we observed that the tumor ECM was able to modulate the monocytes differentiation in favor of M2-like profile. Interestingly, we also revealed that the two components, monocytes and tumor ECM, must be in close proximity, since the ECM-conditioned medium as well as a matrix from healthy tissue did not elicit any effect once applied on monocytes. Tacking advantage from this data we postulate that monocytes release factors that either by acting in the autocrine way or by inducing the release of a ECM component (i.e. fragments of hyaluronic acid), responsible for the decreased of major MHC-II expression. Inspired by these results, we are currently conducting further recellularization experiments that include monocytes to evaluate cell proliferation and treatment response. In conclusion we believe that it is very important to implement our 3D model with cells of the immune compartment and in particular with monocytes and leukocytes in order to re-create a complete cancer model able to mimic the patient's pathology as much as possible.

6.CONCLUSIONS

In conclusion, colon-derived ECMs may likely represent a useful scaffold for assessing the influence of microenvironment in the generation of 3D tumor model able to support cells maintenance, phenotypical preservation and proliferation (1).

Furthermore 3D CRC model represents a preclinical reliable tool to bridge the gap between standard *in vitro* (2D) and *in vivo* (zebrafish) chemosensitivity assays (2).

From the preclinical point of view this system will be suitable for assessing new prognostic drug screening. Thanks to this model it will be possible to evaluate the efficacy of chemotherapeutic agents on tumor cells seeded in their tumor microenvironment and the side effects on cells seeded in the healthy-derived ECM. We are aware of the limitations of the study future analyses will be needed to test the efficacy of several drug treatments and drug combinations on other CRC cell lines but most importantly on patient-derived primary cells in order to combine patient derived scaffold with patient derived cells. Compatibly with the available surgical material, we would like to translate our knowledge in the decellularization and ricellularization protocol using biopsies of pediatric and young-adult patients with the aim of being able to help surgeons and oncologists.

7.ACKNOWLEDGEMENTS

I would like to thank my supervisor Prof. Gianni Bisogno and co-supervisor Marco Agostini.

A great and sincere thanks to Edoardo d'Angelo, Sara Crotti, Sara D'Aronco, and Andrea Biccari from Nano Inspired Biomedicine Lab for their valuable help and support.

Thanks to Martina Piccoli, Diana Corallo and Prof. Piero Pavan, for their precious contribution to this project.

8.REFERENCES

1. Bray, F.; Ferlay, J.; Soerjomataram, I.; Siegel, R.L.; Torre, L.A.; Jemal, A. Global cancer statistics 2018: Globocan estimates of incidence and mortality worldwide for 36 cancers in 185 countries. *CA Cancer J Clin* **2018**, *68*, 394-424.
2. Arnold, M.; Sierra, M.S.; Laversanne, M.; Soerjomataram, I.; Jemal, A.; Bray, F. Global patterns and trends in colorectal cancer incidence and mortality. *Gut* **2017**, *66*, 683-691.
3. Pappo, A.S.; Furman, W.L.; Schultz, K.A.; Ferrari, A.; Helman, L.; Krailo, M.D. Rare tumors in children: Progress through collaboration. *J Clin Oncol* **2015**, *33*, 3047-U3150.
4. Kaatsch, P. Epidemiology of childhood cancer. *Cancer Treat Rev* **2010**, *36*, 277-285.
5. Fearon, E.R.; Vogelstein, B. A genetic model for colorectal tumorigenesis. *Cell* **1990**, *61*, 759-767.
6. De Palma, F.D.E.; D'Argenio, V.; Pol, J.; Kroemer, G.; Maiuri, M.C.; Salvatore, F. The molecular hallmarks of the serrated pathway in colorectal cancer. *Cancers (Basel)* **2019**, *11*.
7. Jasperson, K.W.; Tuohy, T.M.; Neklason, D.W.; Burt, R.W. Hereditary and familial colon cancer. *Gastroenterology* **2010**, *138*, 2044-2058.
8. Liu, Q.; Tan, Y.Q. Advances in identification of susceptibility gene defects of hereditary colorectal cancer. *J Cancer* **2019**, *10*, 643-653.
9. Saab, R.; Furman, W.L. Epidemiology and management options for colorectal cancer in children. *Paediatr Drugs* **2008**, *10*, 177-192.
10. Vasen, H.F.; Moslein, G.; Alonso, A.; Aretz, S.; Bernstein, I.; Bertario, L.; Blanco, I.; Bulow, S.; Burn, J.; Capella, G., *et al.* Guidelines for the clinical management of familial adenomatous polyposis (fap). *Gut* **2008**, *57*, 704-713.
11. Kantor, M.; Sobrado, J.; Patel, S.; Eiseler, S.; Ochner, C. Hereditary colorectal tumors: A literature review on mutyh-associated polyposis. *Gastroenterol Res Pract* **2017**, *2017*, 8693182.
12. Grady, W.M.; Carethers, J.M. Genomic and epigenetic instability in colorectal cancer pathogenesis. *Gastroenterology* **2008**, *135*, 1079-1099.
13. Leslie Sobin, M.G., Christian Wittekind. *Tnm classification of malignant tumours, 7th edition citation*. Wiley-Blackwell: 2009; p 336.
14. Phipps, A.I.; Limburg, P.J.; Baron, J.A.; Burnett-Hartman, A.N.; Weisenberger, D.J.; Laird, P.W.; Sinicrope, F.A.; Rosty, C.; Buchanan, D.D.; Potter, J.D., *et al.* Association between molecular subtypes of colorectal cancer and patient survival. *Gastroenterology* **2015**, *148*, 77-U498.
15. Minsky, B.D.; Cohen, A.M.; Enker, W.E.; Kelsen, D.P.; Kemeny, N.; Frankel, J. Efficacy of postoperative 5-fu, high-dose leucovorin, and sequential radiation therapy for clinically resectable rectal cancer. *Cancer Invest* **1995**, *13*, 1-7.
16. Rothenberg, M.L.; Oza, A.M.; Bigelow, R.H.; Berlin, J.D.; Marshall, J.L.; Ramanathan, R.K.; Hart, L.L.; Gupta, S.; Garay, C.A.; Burger, B.G., *et al.* Superiority of oxaliplatin and fluorouracil-leucovorin compared with either therapy alone in patients with progressive colorectal cancer after irinotecan and fluorouracil-leucovorin: Interim results of a phase iii trial. *J Clin Oncol* **2003**, *21*, 2059-2069.

17. Goyle, S.; Maraveyas, A. Chemotherapy for colorectal cancer. *Digest Surg* **2005**, *22*, 401-414.
18. Saltz, L.B. Adjuvant therapy for colon cancer. *Surg Oncol Clin N Am* **2010**, *19*, 819-+.
19. Carrato, A. Adjuvant treatment of colorectal cancer. *Gastrointest Cancer Res* **2008**, *2*, S42-46.
20. McQuade, R.M.; Stojanovska, V.; Bornstein, J.C.; Nurgali, K. Colorectal cancer chemotherapy: The evolution of treatment and new approaches. *Curr Med Chem* **2017**, *24*, 1537-1557.
21. Indini, A.; Bisogno, G.; Cecchetto, G.; Vitellaro, M.; Signoroni, S.; Massimino, M.; Riccipetitoni, G.; Zecca, M.; Dall'Igna, P.; De Pasquale, M.D., *et al.* Gastrointestinal tract carcinoma in pediatric and adolescent age: The italian trep project experience. *Pediatr Blood Cancer* **2017**, *64*.
22. Rothe, F.; Maetens, M.; Rouas, G.; Paesmans, M.; Van den Eynde, M.; Van Laethem, J.L.; Vergauwe, P.; Deboever, G.; Bareche, Y.; Vandeputte, C., *et al.* Ctcs as a prognostic and predictive biomarker for stage ii/iii colon cancer: A companion study to the pepita trial. *BMC Cancer* **2019**, *19*.
23. Van Cutsem, E.; Cervantes, A.; Nordlinger, B.; Arnold, D. Metastatic colorectal cancer: Esmo clinical practice guidelines for diagnosis, treatment and follow-up. *Ann Oncol* **2014**, *25 Suppl 3*, iii1-9.
24. Kim, H.C.; Kim, C.N.; Yu, C.S.; Roh, S.A.; Kim, J.C. Methylation of the hmlh1 and hmsh2 promoter in early-onset sporadic colorectal carcinomas with microsatellite instability. *Int J Colorectal Dis* **2003**, *18*, 196-202.
25. Ferrari, A.; Bisogno, G.; De Salvo, G.L.; Indolfi, P.; Perilongo, G.; Cecchetto, G.; Trep. The challenge of very rare tumours in childhood: The italian trep project. *Eur J Cancer* **2007**, *43*, 654-659.
26. Bisogno, G.; Ferrari, A.; Bien, E.; Brecht, I.B.; Brennan, B.; Cecchetto, G.; Godzinski, J.; Orbach, D.; Reguerre, Y.; Stachowicz-Stencel, T., *et al.* Rare cancers in children - the expert initiative: A report from the european cooperative study group on pediatric rare tumors. *Klin Padiatr* **2012**, *224*, 416-420.
27. Abbott, R.D.; Kaplan, D.L. Strategies for improving the physiological relevance of human engineered tissues. *Trends Biotechnol* **2015**, *33*, 401-407.
28. Hickman, J.A.; Graeser, R.; de Hoogt, R.; Vidic, S.; Brito, C.; Gutekunst, M.; van der Kuip, H.; Consortium, I.P. Three-dimensional models of cancer for pharmacology and cancer cell biology: Capturing tumor complexity in vitro/ex vivo. *Biotechnology Journal* **2014**, *9*, 1115-1128.
29. Freytes, D.O.; Wan, L.Q.; Vunjak-Novakovic, G. Geometry and force control of cell function. *J Cell Biochem* **2009**, *108*, 1047-1058.
30. Edmondson, R.; Broglie, J.J.; Adcock, A.F.; Yang, L.J. Three-dimensional cell culture systems and their applications in drug discovery and cell-based biosensors. *Assay Drug Dev Techn* **2014**, *12*, 207-218.
31. Kunz-Schughart, L.A.; Freyer, J.P.; Hofstaedter, F.; Ebner, R. The use of 3-d cultures for high-throughput screening: The multicellular spheroid model. *J Biomol Screen* **2004**, *9*, 273-285.
32. Hay, M.; Thomas, D.W.; Craighead, J.L.; Economides, C.; Rosenthal, J. Clinical development success rates for investigational drugs. *Nature Biotechnology* **2014**, *32*, 40-51.

33. Soranzo, C.; Ingrosso, A. A comparative-study of the effects of anthracycline derivatives on a human adenocarcinoma cell-line (lovo) grown as a monolayer and as spheroids. *Anticancer Res* **1988**, *8*, 369-373.
34. Lees, R.K.; Sordat, B.; MacDonald, H.R. Multicellular tumor spheroids of human colon carcinoma origin. Kinetic analysis of infiltration and in situ destruction in a xenogeneic (murine) host. *Experimental cell biology* **1981**, *49*, 207-219.
35. Langmuir, V.K.; McGann, J.K.; Buchegger, F.; Sutherland, R.M. 131i-anticarcinoembryonic antigen therapy of ls174t human colon adenocarcinoma spheroids. *Cancer Res* **1989**, *49*, 3401-3406.
36. Jansen, M.; Dykstra, M.; Lee, J.I.; Stables, J.; Topley, P.; Knick, V.C.; Mullin, R.J.; Duch, D.S.; Smith, G.K. Effect of purine synthesis inhibition on widr spheroids in vitro or on widr or colon 38 tumors in vivo. Complete growth inhibition but not regression. *Biochem Pharmacol* **1994**, *47*, 1067-1078.
37. Mueller-Klieser, W.; Schreiber-Klais, S.; Walenta, S.; Kreuter, M.H. Bioactivity of well-defined green tea extracts in multicellular tumor spheroids. *International journal of oncology* **2002**, *21*, 1307-1315.
38. Mellor, H.R.; Ferguson, D.J.; Callaghan, R. A model of quiescent tumour microregions for evaluating multicellular resistance to chemotherapeutic drugs. *British journal of cancer* **2005**, *93*, 302-309.
39. Mohanty, C.; Fayad, W.; Olofsson, M.H.; Larsson, R.; De Milito, A.; Fryknäs, M.; Linder, S.T. Massive induction of apoptosis of multicellular tumor spheroids by a novel compound with a calmodulin inhibitor-like mechanism. *journal of Cancer Therapeutics and Research* **2013**, *2*.
40. Chen, Y.; Gao, D.; Liu, H.; Lin, S.; Jiang, Y. Drug cytotoxicity and signaling pathway analysis with three-dimensional tumor spheroids in a microwell-based microfluidic chip for drug screening. *Anal Chim Acta* **2015**, *898*, 85-92.
41. Bhat, S.; Kumar, A. Biomaterials and bioengineering tomorrow's healthcare. *Biomatter* **2013**, *3*.
42. Loh, Q.L.; Choong, C. Three-dimensional scaffolds for tissue engineering applications: Role of porosity and pore size. *Tissue Eng Part B-Re* **2013**, *19*, 485-502.
43. Hutmacher, D.W. Scaffolds in tissue engineering bone and cartilage. *Biomaterials* **2000**, *21*, 2529-2543.
44. Lee, Y.S.; Arinzeh, T.L. Electrospun nanofibrous materials for neural tissue engineering. *Polymers-Basel* **2011**, *3*, 413-426.
45. Ma, P.X. Scaffolds for tissue fabrication. *Mater Today* **2004**, *7*, 30-40.
46. Low, W.C.; Rujitanaroj, P.O.; Lee, D.K.; Messersmith, P.B.; Stanton, L.W.; Goh, E.; Chew, S.Y. Nanofibrous scaffold-mediated rest knockdown to enhance neuronal differentiation of stem cells. *Biomaterials* **2013**, *34*, 3581-3590.
47. Carson, J.S.; Bostrom, M.P. Synthetic bone scaffolds and fracture repair. *Injury* **2007**, *38 Suppl 1*, S33-37.
48. Nooeaid, P.; Salih, V.; Beier, J.P.; Boccaccini, A.R. Osteochondral tissue engineering: Scaffolds, stem cells and applications. *J Cell Mol Med* **2012**, *16*, 2247-2270.
49. Casciari, J.J.; Hollingshead, M.G.; Alley, M.C.; Mayo, J.G.; Malspeis, L.; Miyauchi, S.; Grever, M.R.; Weinstein, J.N. Growth and chemotherapeutic response of cells in a hollow-fiber in vitro solid tumor model. *J Natl Cancer Inst* **1994**, *86*, 1846-1852.

50. Rowley, J.A.; Madlambayan, G.; Mooney, D.J. Alginate hydrogels as synthetic extracellular matrix materials. *Biomaterials* **1999**, *20*, 45-53.
51. Mano, J.F.; Silva, G.A.; Azevedo, H.S.; Malafaya, P.B.; Sousa, R.A.; Silva, S.S.; Boesel, L.F.; Oliveira, J.M.; Santos, T.C.; Marques, A.P., *et al.* Natural origin biodegradable systems in tissue engineering and regenerative medicine: Present status and some moving trends. *Journal of the Royal Society Interface* **2007**, *4*, 999-1030.
52. Peppas, N.A.; Hilt, J.Z.; Khademhosseini, A.; Langer, R. Hydrogels in biology and medicine: From molecular principles to bionanotechnology. *Adv Mater* **2006**, *18*, 1345-1360.
53. Magdeldin, T.; Lopez-Davila, V.; Villemant, C.; Cameron, G.; Drake, R.; Cheema, U.; Loizidou, M. The efficacy of cetuximab in a tissue-engineered three-dimensional in vitro model of colorectal cancer. *J Tissue Eng* **2014**, *5*, 2041731414544183.
54. Worthington, P.; Pochan, D.J.; Langhans, S.A. Peptide hydrogels - versatile matrices for 3d cell culture in cancer medicine. *Front Oncol* **2015**, *5*.
55. Hughes, C.S.; Postovit, L.M.; Lajoie, G.A. Matrigel: A complex protein mixture required for optimal growth of cell culture. *Proteomics* **2010**, *10*, 1886-1890.
56. Dorward, H.S.; Du, A.; Bruhn, M.A.; Wrin, J.; Pei, J.V.; Evdokiou, A.; Price, T.J.; Yool, A.J.; Hardingham, J.E. Pharmacological blockade of aquaporin-1 water channel by aqb013 restricts migration and invasiveness of colon cancer cells and prevents endothelial tube formation in vitro. *J Exp Clin Cancer Res* **2016**, *35*, 36.
57. Pereira, J.F.; Awatade, N.T.; Loureiro, C.A.; Matos, P.; Amaral, M.D.; Jordan, P. The third dimension: New developments in cell culture models for colorectal research. *Cell Mol Life Sci* **2016**, *73*, 3971-3989.
58. Zaman, M.H. The role of engineering approaches in analysing cancer invasion and metastasis. *Nat Rev Cancer* **2013**, *13*, 596-603.
59. Chen, Y.; Lin, Y.; Davis, K.M.; Wang, Q.; Rnjak-Kovacina, J.; Li, C.; Isberg, R.R.; Kumamoto, C.A.; Mecsas, J.; Kaplan, D.L. Robust bioengineered 3d functional human intestinal epithelium. *Sci Rep* **2015**, *5*, 13708.
60. Nehete, J.Y.; Bhambar, R.S.; Narkhede, M.R.; Gawali, S.R. Natural proteins: Sources, isolation, characterization and applications. *Pharmacogn Rev* **2013**, *7*, 107-116.
61. D.L.Kaplan. *Introduction to biopolymers from renewable resources.* 1998; Vol. Materials Approach. Springer, Berlin, Heidelberg.
62. Jain, R.K.; Stylianopoulos, T. Delivering nanomedicine to solid tumors. *Nat Rev Clin Oncol* **2010**, *7*, 653-664.
63. Oshikata, A.; Matsushita, T.; Ueoka, R. Enhancement of drug efflux activity via mdr1 protein by spheroid culture of human hepatic cancer cells. *J Biosci Bioeng* **2011**, *111*, 590-593.
64. Pampaloni, F.; Reynaud, E.G.; Stelzer, E.H.K. The third dimension bridges the gap between cell culture and live tissue. *Nat Rev Mol Cell Bio* **2007**, *8*, 839-845.
65. Shakibaei, M.; Kraehe, P.; Popper, B.; Shayan, P.; Goel, A.; Buhrmann, C. Curcumin potentiates antitumor activity of 5-fluorouracil in a 3d alginate tumor microenvironment of colorectal cancer. *BMC Cancer* **2015**, *15*.
66. Ozbolat, I.T. Bioprinting scale-up tissue and organ constructs for transplantation. *Trends in Biotechnology* **2015**, *33*, 395-400.

67. Subia, B.; Dey, T.; Sharma, S.; Kundu, S.C. Target specific delivery of anticancer drug in silk fibroin based 3d distribution model of bone-breast cancer cells. *Acs Appl Mater Inter* **2015**, *7*, 2269-2279.
68. Talukdar, S.; Kundu, S.C. A non-mulberry silk fibroin protein based 3d in vitro tumor model for evaluation of anticancer drug activity. *Adv Funct Mater* **2012**, *22*, 4778-4788.
69. Ozbolat, I.T. Scaffold-based or scaffold-free bioprinting: Competing or complementing approaches? *Journal of Nanotechnology in Engineering and Medicine* **2015**, *6(2)*
70. Knowlton, S.; Onal, S.; Yu, C.H.; Zhao, J.J.; Tasoglu, S. Bioprinting for cancer research. *Trends in Biotechnology* **2015**, *33*, 504-513.
71. Peng, W.J.; Datta, P.; Ayan, B.; Ozbolat, V.; Sosnoski, D.; Ozbolat, I.T. 3d bioprinting for drug discovery and development in pharmaceutics. *Acta Biomaterialia* **2017**, *57*, 26-46.
72. Robbins, J.B.; Gorgen, V.; Min, P.; Shepherd, B.R.; Presnell, S.C. A novel in vitro three-dimensional bioprinted liver tissue system for drug development. *Faseb J* **2013**, *27*.
73. Sensi, F.; D'Angelo, E.; D'Aronco, S.; Molinaro, R.; Agostini, M. Preclinical three-dimensional colorectal cancer model: The next generation of in vitro drug efficacy evaluation. *J Cell Physiol* **2018**, *234*, 181-191.
74. Gilbert, T.W.; Sellaro, T.L.; Badylak, S.F. Decellularization of tissues and organs. *Biomaterials* **2006**, *27*, 3675-3683.
75. Crapo, P.M.; Gilbert, T.W.; Badylak, S.F. An overview of tissue and whole organ decellularization processes. *Biomaterials* **2011**, *32*, 3233-3243.
76. Badylak, S.F.; Taylor, D.; Uygun, K. Whole-organ tissue engineering: Decellularization and recellularization of three-dimensional matrix scaffolds. *Annu Rev Biomed Eng* **2011**, *13*, 27-53.
77. Ott, H.C.; Matthiesen, T.S.; Goh, S.K.; Black, L.D.; Kren, S.M.; Netoff, T.I.; Taylor, D.A. Perfusion-decellularized matrix: Using nature's platform to engineer a bioartificial heart. *Nat Med* **2008**, *14*, 213-221.
78. Ott, H.C.; Clippinger, B.; Conrad, C.; Schuetz, C.; Pomerantseva, I.; Ikonomou, L.; Kotton, D.; Vacanti, J.P. Regeneration and orthotopic transplantation of a bioartificial lung. *Nat Med* **2010**, *16*, 927-U131.
79. Uygun, B.E.; Soto-Gutierrez, A.; Yagi, H.; Izamis, M.L.; Guzzardi, M.A.; Shulman, C.; Milwid, J.; Kobayashi, N.; Tilles, A.; Berthiaume, F., *et al.* Organ reengineering through development of a transplantable recellularized liver graft using decellularized liver matrix. *Nat Med* **2010**, *16*, 814-U120.
80. Urbani, L.; Camilli, C.; Phylactopoulos, D.E.; Crowley, C.; Natarajan, D.; Scottoni, F.; Maghsoudlou, P.; McCann, C.J.; Pellegata, A.F.; Urciuolo, A., *et al.* Multi-stage bioengineering of a layered oesophagus with in vitro expanded muscle and epithelial adult progenitors. *Nat Commun* **2018**, *9*.
81. Pinto, M.L.; Rios, E.; Silva, A.C.; Neves, S.C.; Caires, H.R.; Pinto, A.T.; Duraes, C.; Carvalho, F.A.; Cardoso, A.P.; Santos, N.C., *et al.* Decellularized human colorectal cancer matrices polarize macrophages towards an anti-inflammatory phenotype promoting cancer cell invasion via ccl18. *Biomaterials* **2017**, *124*, 211-224.
82. Halvorsen, T.B.; Seim, E. Association between invasiveness, inflammatory reaction, desmoplasia and survival in colorectal-cancer. *J Clin Pathol* **1989**, *42*, 162-166.

83. Ridky, T.W.; Chow, J.M.; Wong, D.J.; Khavari, P.A. Invasive three-dimensional organotypic neoplasia from multiple normal human epithelia. *Nat Med* **2010**, *16*, 1450-U1137.
84. Chen, H.J.; Wei, Z.B.; Sun, J.; Bhattacharya, A.; Savage, D.J.; Serda, R.; Mackeyev, Y.; Curley, S.A.; Bu, P.C.; Wang, L.H., *et al.* A recellularized human colon model identifies cancer driver genes. *Nature Biotechnology* **2016**, *34*, 845-+.
85. Piccoli, M.; Urbani, L.; Alvarez-Fallas, M.E.; Franzin, C.; Dedja, A.; Bertin, E.; Zuccolotto, G.; Rosato, A.; Pavan, P.; Elvassore, N., *et al.* Improvement of diaphragmatic performance through orthotopic application of decellularized extracellular matrix patch. *Biomaterials* **2016**, *74*, 245-255.
86. Stoletov, K.; Klemke, R. Catch of the day: Zebrafish as a human cancer model. *Oncogene* **2008**, *27*, 4509-4520.
87. Kimmel, C.B.; Ballard, W.W.; Kimmel, S.R.; Ullmann, B.; Schilling, T.F. Stages of embryonic-development of the zebrafish. *Dev Dynam* **1995**, *203*, 253-310.
88. Piccoli, M.; D'Angelo, E.; Crotti, S.; Sensi, F.; Urbani, L.; Maghin, E.; Burns, A.; De Coppi, P.; Fassan, M.; Rugge, M., *et al.* Decellularized colorectal cancer matrix as bioactive microenvironment for in vitro 3d cancer research. *J Cell Physiol* **2018**, *233*, 5937-5948.
89. Dunne, L.W.; Huang, Z.; Meng, W.X.; Fan, X.J.; Zhang, N.Y.; Zhang, Q.X.; An, Z.G. Human decellularized adipose tissue scaffold as a model for breast cancer cell growth and drug treatments. *Biomaterials* **2014**, *35*, 4940-4949.
90. Gu, L.; Mooney, D.J. Biomaterials and emerging anticancer therapeutics: Engineering the microenvironment. *Nat Rev Cancer* **2016**, *16*, 56-66.
91. Lu, W.D.; Zhang, L.; Wu, C.L.; Liu, Z.G.; Lei, G.Y.; Liu, J.; Gao, W.; Hu, Y.R. Development of an acellular tumor extracellular matrix as a three-dimensional scaffold for tumor engineering. *PLoS One* **2014**, *9*.
92. El-Bahrawy, M.; Poulsom, R.; Rowan, A.J.; Tomlinson, I.T.; Alison, M.R. Characterization of the e-cadherin/catenin complex in colorectal carcinoma cell lines. *Int J Exp Pathol* **2004**, *85*, 65-74.
93. Chen, W.D.; Han, Z.J.; Skoletsky, J.; Olson, J.; Sah, J.; Myeroff, L.; Platzer, P.; Lu, S.; Dawson, D.; Willis, J., *et al.* Detection in fecal DNA of colon cancer-specific methylation of the nonexpressed vimentin gene. *J Natl Cancer Inst* **2005**, *97*, 1124-1132.
94. Schmoll, H.J.; Van Cutsem, E.; Stein, A.; Valentini, V.; Glimelius, B.; Haustermans, K.; Nordlinger, B.; van de Velde, C.J.; Balmana, J.; Regula, J., *et al.* Esmo consensus guidelines for management of patients with colon and rectal cancer. A personalized approach to clinical decision making. *Ann Oncol* **2012**, *23*, 2479-2516.
95. Choi, M.S.; Kim, S.H.; Kuh, H.J. Penetration of paclitaxel and 5-fluorouracil in multicellular layers of human colorectal cancer cells. *Oncol Rep* **2011**, *25*, 863-870.
96. Aveic, S.; Corallo, D.; Porcu, E.; Pantile, M.; Boso, D.; Zanon, C.; Viola, G.; Sidarovich, V.; Mariotto, E.; Quattrone, A., *et al.* Tp-0903 inhibits neuroblastoma cell growth and enhances the sensitivity to conventional chemotherapy. *Eur J Pharmacol* **2018**, *818*, 435-448.
97. Changenet-Barret, P.; Gustavsson, T.; Markovitsi, D.; Manet, I.; Monti, S. Unravelling molecular mechanisms in the fluorescence spectra of doxorubicin in

aqueous solution by femtosecond fluorescence spectroscopy. *Phys Chem Chem Phys* **2013**, *15*, 2937-2944.
98. Porzionato, A.; Stocco, E.; Barbon, S.; Grandi, F.; Macchi, V.; De Caro, R. Tissue-engineered grafts from human decellularized extracellular matrices: A systematic review and future perspectives. *Int J Mol Sci* **2018**, *19*.
99. Zhang, H.; Wang, X.; Shen, Z.; Xu, J.; Qin, J.; Sun, Y. Infiltration of diametrically polarized macrophages predicts overall survival of patients with gastric cancer after surgical resection. *Gastric Cancer* **2015**, *18*, 740-750.
100. Italiani, P.; Boraschi, D. From monocytes to m1/m2 macrophages: Phenotypical vs. Functional differentiation. *Front Immunol* **2014**, *5*, 514.
101. Tournigand, C.; Andre, T.; Bonnetain, F.; Chibaudel, B.; Lledo, G.; Hickish, T.; Tabernero, J.; Boni, C.; Bachet, J.B.; Teixeira, L., *et al.* Adjuvant therapy with fluorouracil and oxaliplatin in stage ii and elderly patients (between ages 70 and 75 years) with colon cancer: Subgroup analyses of the multicenter international study of oxaliplatin, fluorouracil, and leucovorin in the adjuvant treatment of colon cancer trial. *J Clin Oncol* **2012**, *30*, 3353-3360.
102. Subbiah, V.; Varadhachary, G.; Herzog, C.E.; Huh, W.W. Gastric adenocarcinoma in children and adolescents. *Pediatr Blood Cancer* **2011**, *57*, 524-527.
103. Mak, I.W.Y.; Evaniew, N.; Ghert, M. Lost in translation: Animal models and clinical trials in cancer treatment. *Am J Transl Res* **2014**, *6*, 114-118.
104. Sultan, I.; Rodriguez-Galindo, C.; El-Taani, H.; Pastore, G.; Casanova, M.; Gallino, G.; Ferrari, A. Distinct features of colorectal cancer in children and adolescents a population-based study of 159 cases. *Cancer-Am Cancer Soc* **2010**, *116*, 758-765.
105. Hill, D.A.; Furman, W.L.; Billups, C.A.; Riedley, S.E.; Cain, A.M.; Rao, B.N.; Pratt, C.B.; Spunt, S.L. Colorectal carcinoma in childhood and adolescence: A clinicopathologic review. *J Clin Oncol* **2007**, *25*, 5808-5814.
106. Poles, G.C.; Clark, D.E.; Mayo, S.W.; Beierle, E.A.; Goldfarb, M.; Gow, K.W.; Goldin, A.; Doski, J.J.; Nuchtern, J.G.; Vasudevan, S.A., *et al.* Colorectal carcinoma in pediatric patients: A comparison with adult tumors, treatment and outcomes from the national cancer database. *J Pediatr Surg* **2016**, *51*, 1061-1066.
107. Laquaglia, M.P.; Heller, G.; Filippa, D.A.; Karasakalides, A.; Vlamis, V.; Wollner, N.; Enker, W.E.; Cohen, A.M.; Exelby, P.R.; Lobe, T. Prognostic factors and outcome in patients 21 years and under with colorectal-carcinoma. *J Pediatr Surg* **1992**, *27*, 1085-1090.
108. Goldberg, J.; Furman, W.L. Management of colorectal carcinoma in children and young adults. *J Pediatr Hematol Oncol* **2012**, *34 Suppl 2*, S76-79.
109. Vlachogiannis, G.; Hedayat, S.; Vatsiou, A.; Jamin, Y.; Fernandez-Mateos, J.; Khan, K.; Lampis, A.; Eason, K.; Huntingford, I.; Burke, R., *et al.* Patient-derived organoids model treatment response of metastatic gastrointestinal cancers. *Science* **2018**, *359*, 920-926.
110. Hanahan, D.; Weinberg, R.A. Hallmarks of cancer: The next generation. *Cell* **2011**, *144*, 646-674.
111. Poltavets, V.; Kochetkova, M.; Pitson, S.M.; Samuel, M.S. The role of the extracellular matrix and its molecular and cellular regulators in cancer cell plasticity. *Front Oncol* **2018**, *8*, 431.
112. Weaver, V.M.; Petersen, O.W.; Wang, F.; Larabell, C.A.; Briand, P.; Damsky, C.; Bissell, M.J. Reversion of the malignant phenotype of human breast cells in three-

dimensional culture and in vivo by integrin blocking antibodies. *J Cell Biol* **1997**, *137*, 231-245.
113. Friedrich, J.; Ebner, R.; Kunz-Schughart, L.A. Experimental anti-tumor therapy in 3-d: Spheroids--old hat or new challenge? *Int J Radiat Biol* **2007**, *83*, 849-871.
114. Cohen, E.; Ophir, I.; Shaul, Y.B. Induced differentiation in ht29, a human colon adenocarcinoma cell line. *J Cell Sci* **1999**, *112 (Pt 16)*, 2657-2666.
115. Allison, S.J.; Sadiq, M.; Baronou, E.; Cooper, P.A.; Dunnill, C.; Georgopoulos, N.T.; Latif, A.; Shepherd, S.; Shnyder, S.D.; Stratford, I.J., *et al.* Corrigendum to "Preclinical anti-cancer activity and multiple mechanisms of action of a cationic silver complex bearing n-heterocyclic carbene ligands" [canc. Lett. 403 (2017) 98-107]. *Cancer Lett* **2018**, *431*, 247.
116. Minchinton, A.I.; Tannock, I.F. Drug penetration in solid tumours. *Nat Rev Cancer* **2006**, *6*, 583-592.
117. Asthana, A.; Kisaalita, W.S. Microtissue size and hypoxia in hts with 3d cultures. *Drug Discov Today* **2012**, *17*, 810-817.
118. Tredan, O.; Galmarini, C.M.; Patel, K.; Tannock, I.F. Drug resistance and the solid tumor microenvironment. *J Natl Cancer Inst* **2007**, *99*, 1441-1454.
119. Nietzer, S.; Baur, F.; Sieber, S.; Hansmann, J.; Schwarz, T.; Stoffer, C.; Hafner, H.; Gasser, M.; Waaga-Gasser, A.M.; Walles, H., *et al.* Mimicking metastases including tumor stroma: A new technique to generate a three-dimensional colorectal cancer model based on a biological decellularized intestinal scaffold. *Tissue Eng Part C Methods* **2016**, *22*, 621-635.
120. Gutierrez-Lovera, C.; Vazquez-Rios, A.J.; Guerra-Varela, J.; Sanchez, L.; de la Fuente, M. The potential of zebrafish as a model organism for improving the translation of genetic anticancer nanomedicines. *Genes-Basel* **2017**, *8*.
121. Swartz, M.A.; Fleury, M.E. Interstitial flow and its effects in soft tissues. *Annual Review of Biomedical Engineering* **2007**, *9*, 229-256.
122. Raiha, M.R.; Puolakkainen, P.A. Tumor-associated macrophages (tams) as biomarkers for gastric cancer: A review.